Novel local fluctuation-preserving upscaling techniques for heterogeneous reaction-transport equation in porous media

Igor Traskunov [a,b,c], Arnulf Latz [*,a,b,c]

[a] Institute of Engineering Thermodynamics, German Aerospace Center (DLR), Pfaffenwaldring 38-40, Stuttgart 70569, Germany
[b] Helmholtz Institute Ulm for Electrochemical Energy Storage (HIU), Helmholtzstraße 11, Ulm 89081, Germany
[c] University of Ulm, Ulm 89069, Germany

ARTICLE INFO

Keywords:
Lithium-ion battery
Microstructure
Homogenization
Battery degradation
Asymptotic analysis
Perturbation methods

ABSTRACT

A body of research in the field of lithium-ion batteries is dedicated to the investigation of the influence on their behavior by the complex microstructure of their porous electrodes. Experimental and numerical studies reported the distinctly localized spatial fluctuations of overpotential and lithium ion concentration which are not observed in the simulation results based on a widely used lithium-ion cell's DFN (Doyle-Fuller-Newman) model. Using a combination of perturbation technique and asymptotic analysis, we rigorously derived the analytical results that explain the fluctuation dynamics that was reported earlier in the microstructure-resolving simulations; importantly, it was theoretically demonstrated that the localized fluctuations generally do not disappear in the homogenization limit which is usually used to justify the use of DFN. We reported new numerical results that proves that the approximations made in our theoretical analysis are indeed applicable to the physical and chemical parameters corresponding to the real lithium-ion cells. Our ansatz may be of use for accurate derivation of DFN-like electrochemistry mathematical models beyond the narrow scope of this report, in particular for the models that accurately account for the cell degradation processes which are sensitive to the particle-scale local environment in the electrode.

1. Introduction

Lithium-ion batteries are complex systems whose behavior depends on the variety of parameters describing the processes on different time and length scales, starting from the molecular transition dynamics defining the standard potentials of the active materials and ending with the thermal and mechanical characteristics of the pack geometry. To achieve computationally efficient modeling, this complexity suggests a multilevel approach in which variations of the solution on the fine scale are averaged out on the coarse scale. An example of such level-to-level transitions is a relation between microstructure resolved electrode models for batteries, that cover the effects on the scale of 10 nm and more, and the models based on the porous electrode theory by Newman and coworkers [1]. The latter treats porous electrodes as homogeneous materials and thus covers the length scales above the local details of their microstructure. The porous electrode theory is significantly more efficient computationally, but it comes at the cost of neglecting a lot of the microstructural details, which might still be relevant for the macroscopic electrochemical behavior of electrodes and making a number of simplifying assumptions, which we will show not to be justified in general.

The porous electrode theory gave rise to a family of DFN models [2–5], which are usually derived from the microscopic model equations using the formal volume-averaging rules [6,7]. The correctness of this procedure was investigated with the help of the homogenization theory, a mathematical ansatz covering the upscaling of partial differential equations [8–10]. As the authors pointed out, the homogenization alone does not suffice for a complete derivation of DFN models: active material ion transport is too slow to satisfy the needed time scale separation condition. Reflecting these circumstances, DFN models employ effective geometrical representations of the microstructure to account for the effects of the active material transport, the most typical one being an effective spherical particle, and solving transport equations for it is an important contributing factor to the computational efficiency.

A number of results were reported that addressed precisely the aspects of the cell dynamics that deviate from the DFN predictions. In [11, 12] one ran the microstructure-resolving numerical simulations based on the phase distribution obtained with X-ray-based electrode

* Corresponding author at: Helmholtz Institute Ulm for Electrochemical Energy Storage (HIU), Helmholtzstraße 11, 89081 Ulm, Germany.
E-mail addresses: igor.traskunov@dlr.de (I. Traskunov), arnulf.latz@dlr.de (A. Latz).

tomography. A local variability in such variables as concentration, current density, OCV, overpotential and intercalation reaction rate was reported there; it is not characteristic of the homogeneous picture of DFN by construction, because in the spherically symmetrical solutions here the localized variability along the phase interface is not possible by definition. The authors of Darling and Newman [13], Ender [14], Schmidt et al. [15] looked specifically at a particular class of DFN modifications in which the local deviations from the classical DFN emerged naturally and systematically. A series of experimental studies based on the optical in situ measurements indicated a presence of local "hot spots" of lithiation [16,17]; here the numerical simulations were presented, based on which the authors argued that the local transport anisotropy in graphite may be a source of the deviations from DFN. Also, based on their numerical and experimental findings, the authors argued that further investigation of the inaccuracies in DFN may be of importance for the correct account of the microstructure-localized cell degradation phenomena. Other experimental techniques hinted at the local lithiation variability [18]. Finally, in Latz and Zausch [19] spatially localized fluctuations of overpotential were reported in the context of a direct comparison between DFN and the microstructure-resolving simulation.

This paper has two main objectives. First, it serves as a continuation of the series [19–21] in which the relation between the DFN accuracy and the local derivation from the homogeneous cell picture were investigated. In [20], we presented numerical analysis of the local fluctuations in the microstructure calculated using the microscopic model derived in Latz and Zausch [19,22]; based on the paper's data and on analytical results, we argued that the local fluctuations do not disappear with homogenization (in contrast, they even become more noticeable as one moves toward high power/high C-rate cell applications), and their emergence and dynamics is due to the local microstructure anisotropy (non-spherical particle shape, additive material distribution, etc.). In [21], we introduced a cell model that is comparable to DFN in terms of computational efficiency but accounts for the local fluctuations with high accuracy (it is based on the linearized eDFN model derived below in the text).

Here we aim at filling the gaps in the presentation above. The theoretical results that were introduced only with heuristic justification will be mathematically rigorously derived, with a specification of the approximations and the assumptions needed and of their limits. The necessary numerical results that assess the applicability of the results and that were missing in the previous contributions will be reported.

The second main objective is to establish a new mathematical analysis method for the partial differential equation problems associated with the lithium-ion cells and similar transport-reaction systems in the porous media, both as a basis for the DFN approximation derivation and as a standalone theoretical analysis tool. The cornerstone of this approach is an asymptotic analysis of the solutions in a quasi-stationary regime, which will be shortly reviewed in general mathematical terms, with a discussion of its possible limitations in other cell models. The general method has, however, the potential to produce more concise yet mathematically accurate extensions of DFN with strong explanatory power beyond the problems covered specifically in this paper, in particularly for the investigation of the upscaling of the microscopic cell models incorporating the side-reactions, the degradation phenomena, as discussed in Harris et al. [17], Latz and Zausch [19], Hein et al. [23].

The paper is organized as follows. In Section 2, we will review the microscopic cell model and DFN. The role of homogenization in connection between these two models will be discussed, together with its limitations. Section 3 outlines the summary of the models and the approximations to be introduced in the following two Sections. Section 4 defines eDFN model, specifies its accuracy and criteria; all the important elements of our mathematical method are introduced here, including the asymptotic analysis and the role of stability. Using Section 4 as a blueprint, Section 5 introduces linearized eDFN as a further approximation of the microscopic model and gives the proof of the localized fluctuation non-disappearance in the homogenization limit corresponding to the classical DFN. Numerical investigation of the accuracy of linearized eDFN is presented. In Section 6, we summarize the main elements of our derivation framework and assess the method's potential and limitations in the development of first principle-based upscaled cell models extending the classical DFN.

2. Different cell models and homogenization

2.1. Microscopic cell model and DFN

Here we review two LIB models: the microscopic model by Latz and Zausch [19] and the corresponding DFN model.

In the microscopic model, the cell is described by a system of partial differential equations (PDEs). The cell is represented by a geometrical domain, split into two subdomains that represent two types of phases: electrolyte (domain "Electrolyte" in Fig. 1, left side) and active material (domain "Active material" in Fig. 1, left side). The equations are defined on these domains, boundary conditions being defined on the domain interfaces to close the system. The state of the cell is defined by four variables-functions of location: lithium ion concentrations c_e and c_s, electrochemical potential ϕ_e, electrical potential Φ_s. The subscript specify the subdomains in which the variables are defined: c_e and ϕ_e in the electrolyte, c_s and Φ_s in the active material. The four equations for the four variables are:

$$\frac{\partial c_e}{\partial t} \quad \vec{\nabla}\vec{N_e}, \tag{1}$$

$$\frac{\partial c_s}{\partial t} \quad \vec{\nabla}\vec{N_s}, \tag{2}$$

$$0 \quad \vec{\nabla}\vec{j_e}, \tag{3}$$

$$0 \quad \vec{\nabla}\vec{j_s}. \tag{4}$$

First two equation are the mass conservation laws for lithium, the remaining two are the charge neutrality constraints. The vector fields $\vec{N}$ and $\vec{j}$ are the flux of lithium and electric current respectively. They are expressed through the system state variables with the following constitutive relations:

$$\vec{j_e} \quad \kappa_e\vec{\nabla}\phi_e \quad \kappa_e\frac{1}{F}\frac{t_+}{}\frac{\partial\mu_e}{\partial c_e}\vec{\nabla}c_e, \tag{5}$$

$$\vec{j_s} \quad \sigma_s\vec{\nabla}\Phi_s, \tag{6}$$

$$\vec{N_e} \quad D_e\vec{\nabla}c_e + \frac{t_+}{F}\vec{j}_e, \tag{7}$$

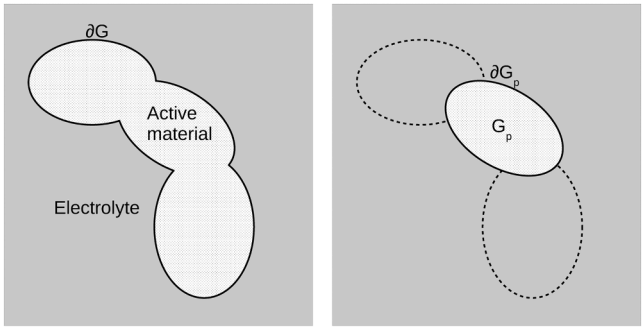

Fig. 1. The domains on which the investigated PDE problems are defined. To the right, the domains and interfaces of the microscopic model in Section 2. To the left, the one-particle domain G_p used to define the standalone problems in Sections 4 and 5.

$$\vec{N_s} \quad D_s \vec{\nabla} c_s. \tag{8}$$

The transport coefficients have the following physical meaning: κ_e is the electrical conductivity of the electrolyte, σ_s is the electrical conductivity the active material, $D_{e,s}$ is the lithium ion diffusion coefficient in the respective phase, t_+ is the lithium ion electrolyte transference number and μ_e is the lithium ion chemical potential in the electrolyte. Some of the coefficients represent the effective collective behavior of few species; their exact meaning in the context of non-equilibrium thermodynamics can be found in Latz and Zausch [19,22].

The four equations for the four variables are supplemented by four boundary conditions on the subdomain interface (∂G in Fig. 1, left side):

$$\vec{j_s} \cdot \vec{n}_{se}\Big|_{\partial G} \quad i_0(c_e, \phi_e, \Phi_s, c_s), \tag{9}$$

$$\vec{j_e} \cdot \vec{n}_{se}\Big|_{\partial G} \quad i_0(c_e, \phi_e, \Phi_s, c_s), \tag{10}$$

$$\vec{N_s} \cdot \vec{n}_{se}\Big|_{\partial G} \quad \frac{i_0(c_e, \phi_e, \Phi_s, c_s)}{F}, \tag{11}$$

$$\vec{N_e} \cdot \vec{n}_{se}\Big|_{\partial G} \quad \frac{i_0(c_e, \phi_e, \Phi_s, c_s)}{F}, \tag{12}$$

where $\vec{n}_{se}$ is a unit normal vector from domain s to domain e. The conditions mean that ions are transferred between phases due to the intercalation-deintercalation reaction whose rate (in terms of electric charge transferred per unit of area per unit of time) is defined by the exchange current function $i_0(c_e, \phi_e, \Phi_s, c_s)$ (or ion flux exchange function $N \quad i_0/F$). We emphasize the state variables on which it depends to compare them with the types of dependence that will occur later in the text. Our analysis rarely relies on a specific functional form of $i_0(\dots)$ explicitly, but its important features may be illustrated by using a type of Butler–Volmer kinetics that was used in Latz and Zausch [19]:

$$i_0 \quad 2i_{00}\sqrt{c_e c_s\left(c_s^{(\max)} \quad c_s\right)}\sinh\left(\frac{F}{2RT}\eta\right), \tag{13}$$

$$\eta \quad \Phi_s \quad U_0(c_s) \quad \phi_e, \tag{14}$$

where we defined the reaction overpotential η through the open circuit potential U_0 of the active material. One important property of $i_0(\dots)$ that will play an important role throughout this paper below is that its slope relative to c_s is (at least almost always) positive:

$$\frac{\partial i_0}{\partial c_s} > 0. \tag{15}$$

One can check by calculating the derivative that in the case of Butler–Volmer formula this property holds as long as the effective chemical potential of lithium (i.e. U_0) satisfies the thermodynamic stability criteria and one can neglect the pre-exponential factor. The latter holds for the OCVs used in the typical electrode active materials, at least for the states of charge (SOC) within the cell operation range.

Additional boundary conditions should be added on the outer boundaries of the domain that specify the cell interactions with the external elements, such as current collectors, electrical circuits and so on. Their exact character is not important in the context of this paper. Yet, when we compare the solutions of different models below, we naturally imply by default that these external factors and their time evolution are well defined and the same in each model.

The second model to be considered is the DFN model. The model is similarly defined through PDEs. It treats the cell components as composite homogeneous materials. Hence the geometrical domain representing the cell splits into subdomains representing the functional components, the separator and the electrodes, not the distinctive chemical phases, as in the microscopic model case. The following cell state functions-variables (for which we use superscript (n), short for "Newman") are defined on these subdomains: $c_e^{(n)}$, $\phi_e^{(n)}$ and $\Phi_s^{(n)}$. The last one is defined only in the subdomains where the active material is present, i.e. the electrodes. The physical meaning of the variables is the same as in the microscopic description above, only in the volume-averaged homogeneous sense. As a special case, the variable describing the lithium concentration in the active material is defined on a 4D domain: $c_s^{(n)}(\vec{x}, r)$. r is a one-dimensional coordinate-distance to the center of an effective sphere of the radius R that represents the active material particles in DFN, $\vec{x}$ is the active material particle location inside the composite electrode. R is chosen to fit the specific surface area of the electrode microstructure.

The following set of PDEs describes the cell evolution:

$$\frac{\partial c_e^{(n)}}{\partial t} \quad \vec{\nabla}\vec{N_e}^{(n)} + \frac{1}{F} a i_0\left(c_e^{(n)}, \phi_e^{(n)}, \Phi_s^{(n)}, c_s^{(n)}|_{r\ R}\right), \tag{16}$$

$$0 \quad \vec{\nabla}\vec{j_e}^{(n)} + a i_0\left(c_e^{(n)}, \phi_e^{(n)}, \Phi_s^{(n)}, c_s^{(n)}|_{r\ R}\right), \tag{17}$$

$$0 \quad \vec{\nabla}\vec{j_s}^{(n)} \quad a i_0\left(c_e^{(n)}, \phi_e^{(n)}, \Phi_s^{(n)}, c_s^{(n)}|_{r\ R}\right), \tag{18}$$

$$\frac{\partial c_s^{(n)}}{\partial t} \quad \frac{1}{r^2}\frac{\partial}{\partial r}\left(D_s r^2 \frac{\partial c_s^{(n)}}{\partial r}\right). \tag{19}$$

The corresponding constitutive relations are:

$$\vec{j_e}^{(n)} \quad \kappa_e^{(eff)} \vec{\nabla}\phi_e^{(n)} \quad \kappa_e^{(eff)} \frac{1 \quad t_+}{F} \frac{\partial \mu_e}{\partial c_e^{(n)}} \vec{\nabla} c_e^{(n)}, \tag{20}$$

$$\vec{j_s}^{(n)} \quad \sigma_s^{(eff)} \vec{\nabla}\Phi_s^{(n)}, \tag{21}$$

$$\vec{N_e}^{(n)} \quad D_e^{(eff)} \vec{\nabla} c_e^{(n)} + \frac{t_+}{F}\vec{j_e}^{(n)}. \tag{22}$$

The coefficients are related to the transport processes on the macroscopic, effective homogeneous medium level, thus the notation with the superscript (eff); a is the specific interface area of the microstructure; $i_0(\dots)$ denotes the reaction current density as in the microscopic model. The Eq. (22) is a one-dimensional diffusion equation for spherically-symmetrical solutions. Inside the electrode, only the variable $c_s^{(n)}$ belongs to a different computational domain than the other variables, hence one needs only one boundary condition to connect the equations:

$$D_s \frac{\partial c_s^{(n)}}{\partial r}\Big|_{r\ R} \quad \frac{i_0\left(c_e^{(n)}, \phi_e^{(n)}, \Phi_s^{(n)}, c_s^{(n)}|_{r\ R}\right)}{F}. \tag{23}$$

Another one comes from the spherical symmetry:

$$D_s \frac{\partial c_s^{(n)}}{\partial r}\Big|_{r\ 0} \quad 0. \tag{24}$$

The above two models describe the basic transport and kinetics of the batteries of the insertion type on microscopic and mesoscopic scale. The mesoscopic DFN model above can partially be obtained by volume averaging (as discussed in the Section 2.2 and in more detail in Vidtst and White [6], Wang et al. [7], Latz and Zausch [19]) from the microscopic model and are needed as references for our new upscaling approach. In principle, similar coupled micro-mesoscale schemes and the methods introduced in this paper below are also applicable to generalizations of the basic battery models due to more complicated physical effects, such as DFN-type model including lithium plating [24], mechanical effects in the active material [25], the microscopic model with lithium plating [23].

We will include comments in the text below on how to generalize our method to include additional physical or chemical processes.

2.2. Microscopic battery model upscaling through homogenization

The question of relation between the microscopic model and DFN is in the focus of the present investigation. In its initial presentation, the DFN model and its underlying concepts were formulated, using concepts from porous electrode theory [1] without using more rigorous upscaling techniques. A formal approach using volume averaging techniques to derive the DFN-type equations can be found in Vidtst and White [6], Wang et al. [7], Latz and Zausch [19]. In general, the DFN class of models represents cell elements as macroscopic composite media, and one interprets the state variables as a volume averaged versions of their local microscopic counterparts inside the different domains of the battery. The volume averaging technique gives differential equations for such averaged quantities starting from exact microscopic expression. For example, Eq. (1) together with the boundary condition (12) will turn into the equation for the averaged concentration $c_e^{(av)}$ of the form

$$\frac{\partial c_e^{(av)}}{\partial t} \qquad \vec{\nabla}\, \vec{N_e}^{(av)} + \frac{1}{F} a i_0^{(av)}. \tag{25}$$

Here, $\vec{N_e}^{(av)}$ and $i_0^{(av)}$ are the properly defined averaged flux and reaction current. The boundary condition is thus transformed into a volume source term. The next step is to assume that these average quantities can be expressed in closed form as functions (or functionals) of only $c_e^{(av)}$ and of the other averaged variables, not of the localized microscopic values. In particularly, for the currents and the fluxes one adopts the upscaled constitutive laws in the form similar to Eqs. (20)–(22); for example, for $\vec{N_e}^{(av)}$:

$$\vec{N_e}^{(av)} \qquad D_e^{(eff)} \vec{\nabla} c_e^{(av)} + \frac{t_+}{F} \vec{j_e}^{(av)}. \tag{26}$$

In such manner, one ends up with the DFN-type equations and subdomains by identifying the DFN state variables $c_e^{(n)}, \ldots$ with $c_e^{(av)}, \ldots$. Note that after these volume-averaging steps, the equation for c_s should still be not averaged but rather substituted with the effective spherical particle PDE problem (19), (23), (24). The DFN model in Latz and Zausch [19] is derived from the microscopic model used in the same paper using volume averaging; the same can be said about the pair of microscopic-DFN models we reviewed in the previous Section.

The conjecture, that the solutions of the equations derived from the volume averaging are actually close to the volume-averaged solutions of the microscopic battery models, should be proven. The authors of Taralova [9], Ciucci and Lai [10] gave examples of how one can do it with the help of the homogenization theory, the facts from the remaining part of this Section are taken from these contributions. In particular, in Taralova [9], the homogenization is applied exactly to the model (1)–(12). The homogenization theory is a mathematical ansatz that demonstrates how PDE problems can be upscaled when there is a length- and time-scale separation. Usually, the physics applications are illustrated using periodic microstructures, but mathematical extensions to the random domains exist as well [26]. In the general homogenization theory approach, one introduces a number of parameters characterizing the PDE problem; among them are the ratios of the microscopic to the macroscopic length and time scales respectively:

$$\delta_1 \qquad \frac{L}{L_0}, \tag{27}$$

$$\delta_2 \qquad \frac{\tau_{micro}}{\tau_{macro}}. \tag{28}$$

Depending on the approximations for the boundary conditions equations, a number of additional parameters may have to be tracked. More details can be found in Taralova [9], Ciucci and Lai [10]. When the parameters are small, the solution of the microscopic battery model can be expanded into perturbation series:

$$\begin{aligned} \phi_e \qquad & \phi_e^{(0)} + \phi_e^{(1)} + \ldots, \\ c_e \qquad & c_e^{(0)} + c_e^{(1)} + \ldots, \\ \Phi_s \qquad & \Phi_s^{(0)} + \Phi_s^{(1)} + \ldots, \\ c_s \qquad & c_s^{(0)} + c_s^{(1)} + \ldots. \end{aligned} \tag{29}$$

The terms with superscript (1) and the following ones scale with powers of the small parameters δ_1 and δ_2. Also, these terms have spatial variability only on the microscopic length scale L, and they are averaged out when one calculates the volume-averaged quantities (e.g. $c_e^{(av)}$). Consequently, only $c_e^{(0)}, \ldots$ contribute to $c_e^{(av)}, \ldots$. The main results of the homogenization theory for the type of PDEs we use are: the equations for the variables with superscript (0) are exactly the volume-averaged equations (like (25)), and the calculation of the averaged fluxes and currents can be done according to the closed-form expressions dependent only on the terms with superscript (0) (like (26)). For example, we will have:

$$\frac{\partial c_e^{(0)}}{\partial t} \qquad \vec{\nabla}\, \vec{N_e}^{(0)} + \frac{1}{F} a i_0^{(av)}, \tag{30}$$

$$\vec{N_e}^{(0)} \qquad D_e^{(eff)} \vec{\nabla} c_e^{(0)} + \frac{t_+}{F} \vec{j_e}^{(0)}. \tag{31}$$

The volumetric source terms (like $a i_0^{(av)}/F$) shall be calculated by simply substituting the variables with superscript (0) into the microscopic reaction kinetic expressions. Also, the homogenization theory gives calculation rules for the effective macroscopic transport coefficients ($D_e^{(eff)}, \ldots$). In the general case, these coefficients, even when isotropic on the microscopic level, can become tensors. It does not affect our results, so we use the scalar notations everywhere in the text for simplicity.

To sum up, given the above identification of $c_e^{(0)}, \ldots$ with the volume-averaged variables, the homogenization theory proves that, when its conditions are fulfilled, the volume-averaged variables do indeed obey the volume-averaged equations. The homogenization conditions do not, however, generally hold for the lithium transport in the solid active material. This fact was pointed out in Taralova [9], Lai and Ciucci [27]. The microscopic time scale τ_{micro} in this case is associated with the diffusion time on the microstructure particle scale, which depends inversely on the diffusion coefficient D_s which can be relatively small. As a result, δ_2 defined in (28) may be not small enough to justify accurate homogenization. The role of the active material non-homogenized local lithium gradient build-up in C-rate-limiting behavior of the cells is exactly one of the phenomena that can be captured by the classical DFN model. The use of a separate lithium transport representation for the active material, such as the effective spherically-symmetrical diffusion according to (19), (23) and (24), is crucial for the DFN model's ability to capture the contribution of solid state diffusion to electrochemical overpotentials.

In the context of using the homogenization in derivation of the macroscopic cell models, there is no obvious way around the limitations due to the slow ion diffusion. In fact, as we demonstrate it below, the drive to reach the maximum available C-rates in the LIB charge-discharge protocols is closely connected to making parameter δ_2 not small. To continue using the volume-averaged equations with a mathematically guaranteed accuracy, the former should remain coupled with the exact microscopic PDE problem (2), (8). Such micro-macro binding calculations are computationally costly relative to the DFN-based ones, which motivates the development of better understanding of the battery model upscaling procedure and of the connected problem of DFN accuracy.

Before we proceed with our theoretical derivation, we write down a number of mathematical expressions for the later use as references. First, we list the equations for the exact homogenized cell model in which the transport in the active material is not homogenized. For the solution of

this model, we keep the notations with superscript (0).

$$\frac{\partial c_e^{(0)}}{\partial t} \quad \vec{\nabla}\,\vec{N_e}^{(0)} + \frac{1}{F} a i_0^{(av)}\left(c_e^{(0)}, \phi_e^{(0)}, \Phi_s^{(0)}\right)\left[c_s^{(0)}\right], \tag{32}$$

$$0 \quad \vec{\nabla}\vec{j_e}^{(0)} + a i_0^{(av)}\left(c_e^{(0)}, \phi_e^{(0)}, \Phi_s^{(0)}\right)\left[c_s^{(0)}\right], \tag{33}$$

$$0 \quad \vec{\nabla}\vec{j_s}^{(0)} \quad a i_0^{(av)}\left(c_e^{(0)}, \phi_e^{(0)}, \Phi_s^{(0)}\right)\left[c_s^{(0)}\right], \tag{34}$$

$$\vec{j_e}^{(0)} \quad \kappa_e^{(eff)} \vec{\nabla}\phi_e^{(0)} \quad \kappa_e^{(eff)} \frac{1}{F} \frac{t_+}{} \frac{\partial \mu_e}{\partial c_e^{(0)}} \vec{\nabla} c_e^{(0)}, \tag{35}$$

$$\vec{j_s}^{(0)} \quad \sigma_s^{(eff)} \vec{\nabla}\Phi_s^{(0)}, \tag{36}$$

$$\vec{N_e}^{(0)} \quad D_e^{(eff)} \vec{\nabla} c_e^{(0)} + \frac{t_+}{F}\vec{j_e}^{(0)}, \tag{37}$$

$$\vec{N_s^{(0)}} \quad D_s \vec{\nabla} c_s^{(0)}, \tag{38}$$

$$\frac{\partial c_s^{(0)}}{\partial t} \quad \vec{\nabla}\vec{N_s^{(0)}}, \tag{39}$$

$$\vec{N_s^{(0)}} \cdot \vec{n}_{se}\Big|_{\partial G} \quad \frac{i_0\left(c_e, \phi_e, \Phi_s, c_s^{(0)}\right)}{F}. \tag{40}$$

$$i_0^{(av)}\left(c_e^{(0)}, \phi_e^{(0)}, \Phi_s^{(0)}\right)\left[c_s^{(0)}\right] \quad \int_{CV} \frac{dS}{S_{CV}} i_0\left(c_e, \phi_e, \Phi_s, c_s^{(0)}\right) \tag{41}$$

The last equation is a calculation rule for the average current $i_0^{(av)}$; the surface integration is done over the part of the interface between the phases located inside a macroscopic control volume CV whose total surface area is S_{CV}. The notation $i_0^{(av)}(\ldots)[c_s^{(0)}]$ emphasizes that the averaged current, although a function of the averaged variables, is a functional of the local c_s distribution in a CV, i.e. mapping from a function space into the set of real numbers. Note that the first three parameters of $i_0(\ldots)$ function in Eqs. (40) and (41) are without a subscript. It means that one has to use the whole series (29) in these expressions. It is different from the model found in Chapter 5 of Taralova [9], where $c_e^{(0)}, \phi_e^{(0)}, \Phi_s^{(0)}$ are used in the boundary condition (40). It technically leaves the model not closed since one has to add equations to calculate the small homogenization correction terms, for example, the so-called auxiliary cell equations (see Taralova [9], Ciucci and Lai [10] for details). They themselves are conditioned on the solutions of the non-homogenized group in the equations, thus making the complete implicit functional interdependencies in the PDE problem hard to grasp. In the next chapter, as a part of the approximation introduced there, we will discuss under which conditions the exact microscopic solutions can be substituted with the variables with indices (0).

Now we introduce a new notation for the electrochemical variables that can be accurately homogenized and write down the model (32)–(41) with its help in a more compact way. c_e, ϕ_e, Φ_s will be components of real coordinate space vector u: $c_e \quad u_1, \phi_e \quad u_2, \Phi_s \quad u_3$. Then PDEs and constitutive laws (32)–(37) can be expressed in the following forms: either

$$\frac{\partial u_i^{(0)}}{\partial t} \quad \vec{\nabla}\left(\sum_j \alpha_{ij} \vec{\nabla} u_j^{(0)}\right) + a N_i^{(av)}\left(u^{(0)}\right)\left[c_s^{(0)}\right] \tag{42}$$

or

$$0 \quad \vec{\nabla}\left(\sum_j \alpha_{ij} \vec{\nabla} u_j^{(0)}\right) + a N_i^{(av)}\left(u^{(0)}\right)\left[c_s^{(0)}\right]. \tag{43}$$

N_i are the fluxes of quantities u_i through the phase interface (either $\pm i$ or i/F in the microscopic model). The corresponding rule of averaging is

$$N_i^{(av)}\left(u^{(0)}\right)\left[c_s^{(0)}\right] \quad \int_{CV} \frac{dS}{S_{CV}} N_i\left(u, c_s^{(0)}\right). \tag{44}$$

The remaining equations are:

$$\frac{\partial c_s^{(0)}}{\partial t} \quad \vec{\nabla}\left(D_s \vec{\nabla} c_s^{(0)}\right), \tag{45}$$

$$D_s \vec{\nabla} c_s^{(0)} \cdot \vec{n}_{se}\Big|_{\partial G} \quad \frac{i_0\left(u, c_s^{(0)}\right)}{F}. \tag{46}$$

The new notation will be used in the text below to keep mathematical expressions more concise. Also, the homogenized model written in such form emphasizes a more general applicability of the theory that we develop than the upscaling of the specific microscopic model (1)–(12). In a more general sense, we wrote down a set of equations describing a class of (electro-)chemical transport-reaction systems in porous media, in which one part of system variable dynamics can be homogenized, and another part not; both sets of variables are still dynamically coupled. Such extensions in the context of battery research is natural when considering, for example, battery systems with more species or/and the phases representing the products of the side reactions.

A further property of the homogenization theory we will need to use below is that the amplitude of variation of the correction terms $u^{(1)}$ in the homogenization perturbation series (29) scales proportionally to the gradients of the homogenized variables $u^{(0)}$:

$$u^{(1)} \sim L\left|\vec{\nabla} u^{(0)}\right|, \tag{47}$$

where L is the microscopic length scale, as in (27).

3. Cell models summary

The presentation in the following Sections will proceed as follows: (1) the mathematical derivation of the cell models, (2) the analysis of the accuracy of the underlying approximations and (3) the use of quasi-stationary solutions of the models to derive the results about the localized fluctuation dynamics. The models are: the extended DFN (eDFN) in

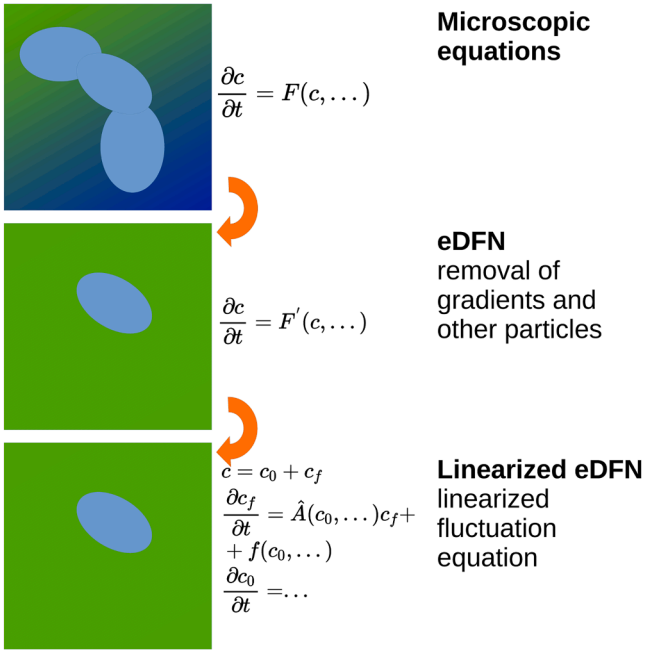

Fig. 2. The summary of the essential features of the considered cell models. It includes the basic assumptions lying behind the approximation used in the derivation in Sections 4 and 5.

Section 4 and the linearized extended DFN (linearized eDFN) in Section 5. Fig. 2 provides a graphical summary of the approximations and the mathematics of the models.

4. Extended DFN (eDFN)

In this Section, we introduce and derive the extended DFN model (eDFN). With eDFN we denote an approximation of the model (42)–(46), defined by two properties: first, in formula (46), u is substituted with the solution of Eqs. (42), (43), and, second, the domain on which the PDE subproblem (45) and (46) is defined, is constraint to just one active material particle, not the whole active material. Although this transition may seem intuitive and trivial, it is interesting to follow it with a level of mathematical rigor. First, there is a methodological value: one will see that the derivation methods are transferable to the further approximations in the rest of the paper; they can potentially be applied to the approximation treating phenomena beyond the present consideration (for example, anisotropic diffusion). Second, as a consequence of the first, the important mathematical results, in particular on the dynamics of the local fluctuations beyond the scope of the classical DFN, are also transferable to the further approximations. Finally, by formulating the conditions under which the transition to eDFN is valid, we can outline the potential areas of the future applications where such transition is not possible.

We will denote the solution of eDFN by letters with superscript (en), short for "extended Newman". The difference between it and the homogenized solution is denoted with superscript $(en,1)$. They are due to variation of c_s along the surface of the active particle and possibly inhomogeneities in the electrolyte on the scale of the particle. Then, one has by definition:

$$u^{(0)} \quad u^{(en)} + u^{(en,1)}, \tag{48}$$

$$c_s^{(0)} \quad c_s^{(en)} + c_s^{(en,1)}. \tag{49}$$

The eDFN equations are:

$$\frac{\partial u_i^{(en)}}{\partial t} \quad \overrightarrow{\nabla}\left(\sum_j \alpha_{ij}\overrightarrow{\nabla}u_j^{(en)}\right) + aN_i^{(av)}\left(u^{(en)}\right)\left[c_s^{(en)}\right] \tag{50}$$

or

$$0 \quad \overrightarrow{\nabla}\left(\sum_j \alpha_{ij}\overrightarrow{\nabla}u_j^{(en)}\right) + aN_i^{(av)}\left(u^{(en)}\right)\left[c_s^{(en)}\right], \tag{51}$$

$$N_i^{(av)}\left(u^{(en)}\right)\left[c_s^{(en)}\right] \quad \int_{CV}\frac{dS}{S_{CV}}N_i\left(u^{(en)}, c_s^{(en)}\right), \tag{52}$$

$$\frac{\partial c_s^{(en)}}{\partial t} \quad \overrightarrow{\nabla}\left(D_s\overrightarrow{\nabla}c_s^{(en)}\right), \tag{53}$$

$$D_s\overrightarrow{\nabla}c_s^{(en)}\cdot\overrightarrow{n}_{pe}\Big|_{\partial G_p} \quad \frac{i_0\left(u^{(en)}, c_s^{(en)}\right)}{F}. \tag{54}$$

We introduced domain G_p as a part of space occupied by one particle (see Fig. 1, right side). $\overrightarrow{n}_{pe}$ is a unit normal vector directed outside of this domain. Where the particle faces the electrolyte phase, it is identical to $\overrightarrow{n}_{se}$. On the part of the particle interface that faces other particles, we set by definition $i_0 \quad 0$. Although one has to keep in mind that the microstructure consists of many particles, we do not introduce indexing separating G_p of the different particles since it is not important for the derivation.

Let us now formulate the perturbation equations governing the evolution of the difference, starting with the equations for $c_s^{(en,1)}$. We assume that the difference is small enough so that only the following terms of the Taylor expansions of $i_0(\ldots)$ should be kept:

$$i_0\left(u, c_s^{(0)}\right) \quad i_0\left(u^{(en)}, c_s^{(en)}\right) + \\ + \sum_i \frac{\partial i_0}{\partial u_i}\left(u^{(en)}, c_s^{(en)}\right)\cdot\left(u_i^{(en,1)} + u_i^{(1)}\right) + \\ \beta\left(u^{(en)}, c_s^{(en)}\right)\cdot c_s^{(en,1)} + \ldots, \tag{55}$$

$$\beta(\ldots) \quad \frac{\partial i_0}{\partial c_s}(\ldots). \tag{56}$$

The neglected terms are smaller than the $u_i^{(1)}$ perturbation corrections in the homogenization theory expansion (29). Using (55), we subtract (53) and (54) from (45) and (46) respectively. Then we have:

$$\frac{\partial c_s^{(en,1)}}{\partial t} \quad \overrightarrow{\nabla}\left(D_s\overrightarrow{\nabla}c_s^{(en,1)}\right), \tag{57}$$

$$D_s\overrightarrow{\nabla}c_s^{(en,1)}\cdot\overrightarrow{n}_{pe}\Big|_{\partial G_p} \quad \frac{1}{F}\beta\left(u^{(en)}, c_s^{(en)}\right)\cdot c_s^{(en,1)} + \\ + \sum_i \frac{1}{F}\frac{\partial i_0}{\partial u_i}\left(u^{(en)}, c_s^{(en)}\right)\cdot\left(u_i^{(en,1)} + u_i^{(1)}\right) + \\ + N_{ip} + \ldots. \tag{58}$$

Note that here, and elsewhere in the text, we neglect the dependence of the transport coefficients $(D_s, \ldots)$ on the state variables c and u. Their inclusion will not affect the validity of our approach in general but would require introduction of additional small parameters. N_{ip} is a lithium flux through the interparticle interface; on the other parts of G_p $N_{ip} \quad 0$.

4.1. The role of stability in the perturbation term equations

We rewrite the perturbation PDE problem in the following concise form:

$$\frac{\partial c_s^{(en,1)}}{\partial t} \quad \overrightarrow{\nabla}\left(D_s\overrightarrow{\nabla}c_s^{(en,1)}\right), \tag{59}$$

$$D_s\overrightarrow{\nabla}c_s^{(en,1)}\cdot\overrightarrow{n}_{pe}\Big|_{\partial G_p} \quad \frac{\beta}{F}c_s^{(en,1)} + \delta N, \tag{60}$$

$$\delta N \quad \sum_i \frac{1}{F}\frac{\partial i_0}{\partial u_i}\left(u^{(en)}, c_s^{(en)}\right)\cdot\left(u_i^{(en,1)} + u_i^{(1)}\right) + N_{ip} + \ldots. \tag{61}$$

Thus we grouped together the terms that depend on $c_s^{(en)}$ and the ones that do not. It is instrumental for this Subsection, in which we discuss a number of the PDE system's properties which are relevant for the further analysis and will be used as a reference below.

The properties arise from the stability characteristics of the PDE system treated as a dynamical system. Only the necessary facts will be summarized here. To get acquainted with a detailed explanation of the subject, accurate proofs and more rigorous definitions beyond the scope of this summary, the reader can be referred to textbooks on mathematical physics and dynamical systems (for example [28,29]). To make the necessary definitions, we write down the initial value problem for a general dynamic system as

$$\frac{d\overrightarrow{x}}{dt} \quad \overrightarrow{F}\left(\overrightarrow{x}, \overrightarrow{\theta}\right), \tag{62}$$

$$0 \quad \overrightarrow{G}\left(\overrightarrow{x}, \overrightarrow{\theta}\right), \tag{63}$$

$$\overrightarrow{x}(t \quad 0) \quad \overrightarrow{x}_0. \tag{64}$$

Here the state of the dynamical system is described by vector variable $\overrightarrow{x}$. For the system (59) and (60), $\overrightarrow{x}$ corresponds to a vector from the linear

space of all possible functions $c_s^{(en,1)}(\vec{x})$ on the PDE problem domain (with additional mathematical constraints to allow existence of the differentiation operators in PDEs). $\vec{\theta}$ denotes the dynamical system parameters. Generally, they can explicitly depend on time. The boundary conditions (60) without explicit time differentiation can be treated as a particular case of (63). The latter can be formally treated as a projection of the trajectories $\vec{x}(t)$ on a manifold in the state space defined by (63) and can be dropped with a help of state variable redefinition. We keep it to preserve the formal correspondence to (59) and (60).

Equilibrium of the dynamical system (62) and (63) is a solution of 0 $\vec{F}(\vec{x}, \vec{\theta})$. The equilibrium is called Lyapunov stable if, for every initial condition (64) close enough to the equilibrium, the whole trajectory will stay close to it. A more strong equilibrium property is called asymptotic stability: it holds when all the trajectories starting from the initial conditions close enough to the equilibrium eventually converge to it with time.

Later in the text, we will make use of Lyapunov's second method for stability, also known as Lyapunov function method. A smooth enough function of state variable $V(\vec{x})$ in a vicinity of an equilibrium $\vec{x}_{eq}$ is called Lyapunov function when $V(\vec{x}_{eq})$ 0, $V(\vec{x}) > 0$ everywhere else. One can prove that the equilibrium is stable if a Lyapunov function with

$$\frac{dV}{dt} \geq 0 \tag{65}$$

along the trajectory can be found. If one can guarantee the exact $>$ sign, the equilibrium is asymptotically stable.

Another type of stability relevant to our derivation is structural stability. Contrary to the definitions above, this is not a property of an equilibrium state but of a trajectory and of a parameter set value $\vec{\theta}_0$: structural stability exists if, for any set of parameters $\vec{\theta}$ sufficiently close to $\vec{\theta}_0$, the solution of (62)–(64) always remains as close as necessary to the solution with $\vec{\theta}_0$. Structural stability may be thought of as a type of continuity in a space of trajectories with respect to their parameters.

In the application to (59) and (60), having named $c_s^{(en,1)}$ a dynamical system state variable, we will formally treat the other functions entering the equations as the parameters $\vec{\theta}$: δN, D_s, β. In such settings, the following statements about the problem of the type (59) and (60) are valid: if β is positive at least somewhere on the interface and non-negative everywhere (see the discussion of the condition (15) above), there is a unique equilibrium solution and this solution is asymptotically stable. It obeys the stationary PDE problem:

$$0 \quad \vec{\nabla}\left(D_s \vec{\nabla} c_s^{(en,1)}\right), \tag{66}$$

$$D_s \vec{\nabla} c_s^{(en,1)} \cdot \vec{n}_{pe}\Big|_{\partial G_p} \quad \frac{\beta}{F} c_s^{(en,1)} + \delta N. \tag{67}$$

Under the same constraints imposed on β, the solution of the stationary system depends continuously on δN, D_s, β. This property, combined with the asymptotic stability and the system's linearity, allows to prove the structural stability of (59) and (60).

These properties lead to a few useful statements about the dynamical evolution of the terms $c_s^{(en,1)}$. Let us start with the artificial case in which the parameters δN, D_s, β stay constant. Then the solution evolves toward the equilibrium and stays here. Heuristically, the time constant of this convergence is of the order of the diffusion time for the particle size (based on the spectral analysis [28,30]). If one instead considers the situation in which δN, D_s, β change adiabatically, i.e. on a time scale slow enough relative to this equilibration, then the dynamic $c_s^{(en,1)}$ profile tends to stay close to the instant solution of (59) and (60).

For the analysis below, we will assume that this adiabatic dynamics condition holds and will use the solution of the stationary PDE problem as a proxy for the real dynamics. The extent to which it is actually fulfilled for the solution of the model (32)–(41) is hard to pin down in simple mathematical terms, as with the criteria based on parameters (27) and (28). The actual dynamics of δN, D_s, β can be obtained only by solving the complete cell model; potentially, the other equations can induce the effects on specific time scales, and they can influence this dynamics. Eventually, numerical tests should provide the ultimate answer to the question of the approximation applicability; our results in Traskunov and Latz [20,21] implicitly provide such tests and support the closeness of the dynamic solution to the stationary one in the practically relevant cases.

One important candidate for the role of a macro-parameter that will likely influence the stationary solution approximation is the cell C-rate. Intuitively, the faster one charges the cell, the higher is the rate with which various quantities change, including the ones relevant for the needed approximation. It means, the approximation will likely break when the C-rate goes above a certain limit. As one will see below, mathematical criteria bound with C-rate will enter the further derivation below, thus making it an important parameter for the whole topic of DFN accuracy addressed in this paper.

4.2. Properties of the stationary solutions, fluctuation dynamics laws

Based on the role of the stationary solutions of the problem (59) and (60) that was established in the previous Subsection, here we will concentrate exclusively on their properties. The key parameters influencing the dynamics of $c_s^{(en,1)}$ and the related microstructure-localized fluctuations will emerge.

To this end, let us first separate the dimensionless components of the parameters; this procedure will identify specifically the parameters that describe the particle anisotropy from the rest. The first group of the new dimensionless parameters is:

$$\begin{array}{ll} \widetilde{\beta} & \beta/\overline{\beta}|_S, \\ \widetilde{\delta N} & \delta N/\overline{\delta N}|_S, \\ \widetilde{D_s} & D_s/\overline{D_s}|_V, \\ \widetilde{\vec{x}} & \vec{x}/L. \end{array} \tag{68}$$

L is the particle length scale, here defined through the volume and the surface area of the particle domain: L V/S. We use the same notation as the one for the microscopic length scale in Section 2.2. In the text, we assume that this length scale is of the same order as the particle size, so blending them together should not create an ambiguity in the notation. $\widetilde{\vec{x}}$ are dimensionless coordinates; after such coordinate transformation, the original domain of the PDE problem transforms into a geometrically similar one but with L 1. The symbols with horizontal bars mean the parameter average, on the surface and in the volume, as defined by the signs $|_S$ and $|_V$ respectively. Below, we will assume $\overline{\delta N}|_S$ / 0. The opposite requires choosing another measure of the perturbation δN scale but does not change the essentials of our mathematical methods and the conclusions coming from them: as one shall see below, $\overline{\delta N}|_S$ / 0 plays the role of the integral perturbation current scale measure; in singular cases, another choice of the measure that is not zero is possible. The parameters in (68) together with the domain/particle shape described in $\widetilde{\vec{x}}$ coordinates, can be understood as a complete characteristic of the local microstructure inhomogeneity and/or anisotropy. The remaining parameters can be then said to describe the role of total C-rate, reaction kinetics and particle size.

One such dimensionless parameter emerges when one substitutes (68) into the PDE problem:

$$\rho \quad \frac{\overline{\beta}|_S \cdot L}{F \cdot \overline{D_s}|_V}. \tag{69}$$

ρ will play an important role in the theoretical presentation that will

follow. It's instructive to give its basic interpretation as a ratio of two rates or, alternatively, of two characteristic time scales (with a mathematically more sophisticated analysis being given later):

$$\begin{aligned} &\rho \quad \tau_2/\tau_1, \\ &1\Big/\tau_1 \quad \frac{\overline{\beta}|_S}{F\cdot L}, \\ &1\Big/\tau_2 \quad \frac{\overline{D_s}|_V}{L^2}. \end{aligned} \tag{70}$$

τ_2 is a characteristic diffusion time that measures how fast the lithium concentration inhomogeneities are destroyed by diffusion. τ_1 measures how fast the concentration inhomogeneities on the interface decrease due to their negative feedback on the reaction rate measured by $\overline{\beta}|_S$. To see the latter, consider two regions inside the particle near the interface with the volume of order L^3, the surface area of order L^2 and separated by the distance of order L. The concentration difference between them is δc_s. Assuming that a decrease in the concentration growth between the regions may occur only due to the reaction rate difference $\overline{\beta}|_S\cdot\delta c_s$ and thus neglecting any diffusion exchange, one can write an approximate mass balance equation as

$$\frac{\partial \delta c_s}{\partial t}L^3 \sim \frac{\overline{\beta}|_S}{F}\delta c_s L^2. \tag{71}$$

From this, one retrieves the rate constant τ_1:

$$\frac{\partial \delta c_s}{\partial t}\cdot\frac{1}{\delta c_s} \sim \frac{1}{\tau_1} \quad \frac{\overline{\beta}|_S}{F\cdot L}. \tag{72}$$

Using the parameter ρ, we rewrite the stationary PDE problem as:

$$0 \quad \widetilde{\overrightarrow{\nabla}}\left(\widetilde{D_s}\widetilde{\overrightarrow{\nabla}}c_s^{(en,1)}\right), \tag{73}$$

$$\widetilde{D_s}\widetilde{\overrightarrow{\nabla}}c_s^{(en,1)}\cdot\overrightarrow{n}_{pe}\Big|_{\partial G_p} \quad \widetilde{\beta}\cdot\rho\cdot c_s^{(en,1)} + \widetilde{\delta N}\cdot\frac{L\cdot\overline{\delta N}|_S}{\overline{D_s}|_V}. \tag{74}$$

Operator $\widetilde{\overrightarrow{\nabla}}$ denotes differentiation in the dimensionless coordinates. One can see, indeed, that all the parameters with physical dimensions are grouped together into an only one. Few words should be said about the meaning of the separation of the dimensionless parameters and their role. One can say that the ones defined in (68) encode the local microstructure-dependent inhomogeneity and anisotropy. Also, the transformation to the domain with $L \quad V/S \quad 1$ separates the particle size effects from the particle shape effects. The domain shape can be considered as a particle meta-parameter. Although the set of thus defined possible parameters has a structure of functional space, in many practical applications, one can use compressed representations. In this regard, it is useful to mention another heuristic property of the elliptic boundary PDE problems of (73) and (74)-type: the solution sensitivity to local features decreases with their size. Because of this, one can encode the corresponding functions in a way that favors capturing only geometrically large details. One of such representations is the reduced-order LIB model we introduced in Traskunov and Latz [21], in which all the dimensionless parameters are described by a finite set of numbers grouped into matrices. Another example is the encoding of the particle shape with spherical harmonics; a comparison of the model (1)–(12) implementations on the microstructure obtained with tomography and on its artificial twin generated with an algorithm based on such representation can be found in Hein et al. [31].

More insights into the physical meaning of the parameter ρ from (69) can be gained by investigating its influence on the PDE solution. First, due to the problem being linear, one can immediately write it in the form

$$c_s^{(en,1)} \quad \frac{L\cdot\overline{\delta N}|_S}{\overline{D_s}|_V}\cdot f(\widetilde{\vec{x}}, \rho, \ldots), \tag{75}$$

where, with the ellipsis sign, we referred to the dependence on all the remaining parameters, expressed in a compressed form if necessary. More specific expressions can be obtained in asymptotic cases. Let us expand $f(\ldots)$ into power series of $1/\rho$, to identify the solution behavior when $\rho \to +\infty$:

$$f \quad \sum_{n\ 0}^{\infty}\frac{f_n}{\rho^n}. \tag{76}$$

Substituting it into (73)–(73) gives a sequence of PDE problems for f_n. The differential equation is always

$$0 \quad \widetilde{\overrightarrow{\nabla}}\left(\widetilde{D_s}\widetilde{\overrightarrow{\nabla}}f_n\right). \tag{77}$$

The boundary condition for f_0 is $f_0|_{\partial G_p} \quad 0$, where β is not zero, and zero normal flux everywhere else. It means f_0 is zero everywhere in the particle. The subsequent boundary conditions are:

$$\widetilde{\beta}\cdot f_1|_{\partial G_p} \quad \widetilde{\delta N}, \tag{78}$$

$$\widetilde{\beta}\cdot f_n|_{\partial G_p} \quad \widetilde{D_s}\widetilde{\overrightarrow{\nabla}}f_{n\ 1}\cdot\overrightarrow{n}_{pe}, n > 1. \tag{79}$$

One can see that, when $\rho \to +\infty$, the stationary solution asymptotically scales as

$$c_s^{(en,1)} \sim \frac{L\cdot\overline{\delta N}|_S}{\overline{D_s}|_V}\frac{1}{\rho}. \tag{80}$$

To investigate the behavior when $\rho \to +0$, one cannot simply expand f into a series of non-negative powers of ρ: it may lead to PDE problems that have no solutions. Thus, f is not always an analytical function in the vicinity of $\rho \quad 0$. This singularity is related to the fact that problem (59) and (60) may not have a stationary solution when $\beta \quad 0$ (and consequently $\rho \quad 0$). We will search for the solution in the form

$$f \quad g + \sum_{n\ 0}^{\infty} f_n\rho^n, \tag{81}$$

where g is a constant (as function of coordinates) that is chosen in a such way as to ensure that the PDE problems for f_n have solutions. To make it well defined, one has to impose an additional constraint:

$$\int_{\partial G_p} dS\widetilde{\beta}f_n \quad 0. \tag{82}$$

The necessary and sufficient condition that the problem (73) and (74) has a solution is that the surface integral of the right side of (74) over the whole domain boundary is equal to zero [28]. If we chose

$$g \quad \frac{1}{\rho} \tag{83}$$

then substitution of (81) into problem (73) and (74) gives the following sequence of boundary conditions:

$$\widetilde{D_s}\widetilde{\overrightarrow{\nabla}}f_0\cdot\overrightarrow{n}_{pe}\Big|_{\partial G_p} \quad \widetilde{\delta N} \quad \widetilde{\beta}, \tag{84}$$

$$\widetilde{D_s}\widetilde{\overrightarrow{\nabla}}f_n\cdot\overrightarrow{n}_{pe}\Big|_{\partial G_p} \quad \widetilde{\beta}\cdot f_{n\ 1}, n > 0. \tag{85}$$

All f_n obey Eq. (77). Definitions (68) and constraints (82) guarantee that the solutions exist. Moreover, with (82) the solutions are unique. Unlike the case of $\rho \to +\infty$, f_0 is not zero in general.

Having looked at the main asymptotic cases, when $\rho \to +\infty$ and $\rho \to +0$, we are equipped with instruments to investigate the role of ρ deeper. In the former case, the asymptotic solution (80) expressed in the

parameters with physical dimension $c_s^{(en,1)}$ obeys the boundary condition

$$c_s^{(en,1)}|_{\partial G_p} \quad \frac{\delta N}{\beta}. \tag{86}$$

It is a solution of equation

$$0 \quad \delta N + \beta \cdot c_s^{(en,1)} \tag{87}$$

everywhere on the interface. The right side is the total change of the lithium flux (or, multiplied by F, the current density): δN is the part caused by the factors external to the level of active material lithiation (connection/disconnection of the other particles, introduction of a perturbation in u), $\beta \cdot c_s^{(en,1)}$ is the reaction feedback due the introduced changes in $c_s^{(en,1)}$. Thus, when externally perturbed and in the regime with large ρ, the transport-reaction system (53) and (54) tends to react with almost an exact compensation of the perturbation, effectively imposing (87) as a stiff constraint on the dynamics. Moving from the mathematics to a physics-/chemistry-based interpretation, one can say that the reaction rate feedback to an additional accumulation of the reaction products or to an additional depletion of the reactants is faster than the mass transport's one; one can call it a "slow diffusion" regime. Note that the diffusion coefficient does not even enter the expression for $c_s^{(en)}$ on the surface. In the opposite situation of $\rho \to +0$, the asymptotic solution is a sum of two terms. The first one, originating from (83), although depends on ρ, is a constant in the particle domain as a function of coordinates. It represents the overall shift in the average amount of lithium due to the perturbation δN and can become unbounded when the system has a weak negative feedback with ρ being close to zero. The second term comes from f_0, does not depend on ρ and represents local concentration gradient perturbation, along the surface and in the direction perpendicular to it. Since only f_0 and the higher order f_n contribute to the surface fluctuations, one can write an estimate for such fluctuations $\delta c_s|_S$ in the following form with the physical dimensions:

$$\delta c_s|_S \sim \frac{L \cdot \overline{\delta N}|_S}{\overline{D_s}|_V} f^{(1)}(\rho). \tag{88}$$

Here, $f^{(1)}$ is a function of ρ without a singularity at $\rho \quad 0$. In [20], the formulas and the associated comments at the end of Subsection 2.3 directly follow from this fact. To sum up, one can call the case $\rho \to +0$ a "fast diffusion" regime. Correspondingly, β disappears from this limiting case.

Through these observations, one recovers a role for parameter ρ defined in (69): it assesses the relative role of transport and interface reactions in creating a concentration profile near the particle surface. Note that a similar parameter was introduced in the theory of liquid NMR relaxation in porous media in Brownstein and Tarr [30], to separate the slow and the fast diffusion regimes in that context.

Final mathematics-related remarks should be done regarding the terms we dropped from the expansion (61). In principle, one can write a series of PDE problems in the form (59), (60), where the new flux perturbation δN consists of the dropped terms, which can in turn depend on the solutions of the lower order PDE problems (because of the inclusion of the higher power terms for $c_s^{(en,1)}$ from the Taylor series). If one can guarantee that each new correction of δN is significantly smaller than the previous one then their contribution can be neglected altogether. Our numerical analysis in Traskunov and Latz [20,21] suggests that it reliably holds for the typical LIB components and particle sizes. Also, neither of the perturbation terms are the so-called secular terms, i. e. the terms which, however small during a period of time, can grow in an unbounded manner; to the contrary, all the terms tend to fluctuate around the stationary solutions, as long as one can guarantee non-negativity of β and its positivity at least in some parts of the interface. A potential exclusion from this rule, the singularity near $\beta \quad 0$, although not observable numerically in Traskunov and Latz [20], probably due to the smallness of δN compensating the smallness of β, should in principle be accounted for when one develops computational models relying on the results in this text. Importantly, in the Butler–Volmer kinetics (13) utilized in Traskunov and Latz [20], one can demonstrate analytically that δN due to the local gradient in the electrolyte and β become small together excluding the SOC very close to either 0% or 100%.

4.3. *Extended DFN: model applicability criterion, structural stability of the model*

With the help of the obtained results, we can now estimate how close the solution of the homogenized eDFN equation in the form (50) or (51) is to the solution of (42) or (43) when the assumptions made there are fulfilled. Similarly to the treatment of $c_s^{(en,1)}$ above, one can write down the equations for $u^{(en,1)}$ by subtracting (50) from (42) (or, alternatively, (51) from (43)). Omitting the details, one will come to the conclusion that $u^{(en,1)}$ is significantly small relative to $u^{(en)}$ or $u^{(0)}$ when the averaged additional interfacial fluxes

$$\delta N^{(av,1)} \quad \int_{CV} \frac{dS}{S_{CV}} \frac{\partial N}{\partial c_s} \cdot c_s^{(en,1)} \quad \int_{CV} \frac{dS}{S_{CV}} \frac{1}{F} \beta \cdot c_s^{(en,1)}, \tag{89}$$

which emerge as the source term in the equations for $u^{(en,1)}$, are much smaller than $N^{(av)}$ defined by (52) (or, equivalently, by (44)). Thus we defined another important small parameter

$$\delta_3 \quad \frac{\delta N^{(av,1)}}{N^{(av)}}. \tag{90}$$

Taking the comments from Section 4.1 about the relation between the dynamics of $c_s^{(en,1)}$ and the stationary solutions of (66) and (67) into account, one can reliably use the latter in estimating δ_3. Using (75) and definition (69), one obtains

$$\delta_3 \sim \beta \frac{L \cdot \overline{\delta N}|_S}{F \overline{D_s}|_V N^{(av)}} f^{(2)}(\rho) \sim \frac{\overline{\delta N}|_S}{N^{(av)}} \rho f^{(2)}(\rho), \tag{91}$$

where $f^{(2)}(\rho)$ is a dimensionless function coming from the surface averaging of $f(\rho, \ldots)$ in the CV. Obviously, the asymptotic properties relative to ρ are not affected by this averaging. Then, taking the behavior of f at $\rho \to +\infty$ and $\rho \to +0$ into account, we come to the conclusion that $\rho f^{(2)}(\rho)$ always remains bounded. Thus, the smallness of δ_3 is mainly controlled by the ratio of the fluxes

$$\delta_3 \sim \frac{\overline{\delta N}|_S}{N^{(av)}}. \tag{92}$$

We defined eDFN as a model in which we neglect the influence of the local gradients of u and of the direct interparticle lithium exchange. These two factors are presented in the definition of δN in formula (61). Let us now investigate how they influence δ_3.

First, we look at the role of the local gradients of u. The corresponding part of δN is

$$\sum_i \frac{1}{F} \frac{\partial i_0}{\partial u_i} \left(u_i^{(en,1)} + u_i^{(1)} \right). \tag{93}$$

$u_i^{(en,1)}$ should be neglected because it itself comes from the further correction of eDFN whose smallness we try to estimate with δ_3. $u_i^{(1)}$ can be estimated using (47). We obtain

$$\delta_3 \sim \sum_i \frac{\frac{\partial i_0}{\partial u_i} L \left| \vec{\nabla} u_i^{(0)} \right|}{i_0^{(av)}}. \tag{94}$$

δ_3 is small as long as the variation of the reaction current inside the CV due to the local gradients of homogenized solution $u^{(0)}$ is much smaller

than the average current itself. Interestingly, this condition is not independent from the homogenization conditions under which the model (42)-(46) was derived. Indeed, in Taralova [9], the relative smallness of this reaction current variation plays an important role in assigning the homogenization asymptotic expansion orders to various terms in the microscopic cell model equations. Another way to look at the definition of δ_3 is as an implicit necessary condition for the correctness of the treatment of the particle size L as small given the all the other quantities all of which can be estimated from the homogenized model.

In the case of interparticle lithium exchange, we assume that only a small part of the particle surface area belongs to the interparticle interfaces. Its surface area is S_{ip}. In the narrow context of this Subsection, we treat N_{ip} as a characteristic interparticle flux in the areas of connection, not as an exact function, so we do not need additional notations. Then, following the definition of $\overline{\delta N}|_S$, one can write for the contribution of N_{ip} to it:

$$\overline{\delta N}|_S \sim \frac{S_{ip}}{S} N_{ip}; \tag{95}$$

and for the corresponding contribution to δ_3:

$$\delta_3 \sim \frac{S_{ip} \cdot N_{ip}}{S \cdot N^{(av)}}. \tag{96}$$

The small parameter is proportional to the ratio of the total amount of lithium directly exchanged between the particles per unit of time to the total amount of lithium intercalated per unit of time. One can make further estimations, but it requires knowledge about the kinetic laws defining N_{ip}. Here we want to concentrate on the case in which it is defined by the same Fick's law (8) as inside every individual particle. The choice is due to the fact that in Latz and Zausch [19] the electrode active material microstructure's digital representation was constructed by creating direct overlaps between the particles, thus treating it as a continuous domain without interruptions. Aiming at explaining the local fluctuations in overpotential observed in Latz and Zausch [19], we relied on the results of eDFN that we derive below; in this derivation, active material domain representation as a single particle is somewhat crucial. It makes the estimation of the role of N_{ip} a necessary step. Defining l_{ip} as a typical length scale of the region of the particle connection (it can be estimated as $\sim \sqrt{S_{ip}}$), Δc_{ip} as a change of lithium concentration over the region, we write down based on the Fick's law:

$$N_{ip} \sim \frac{D_s \Delta c_{ip}}{l_{ip}} \sim \frac{D_s \Delta c_{ip}}{\sqrt{S_{ip}}}. \tag{97}$$

At this point, we have to refer to the results we will derive below but without dependence on this section: according to formula (129), the variation of concentration inside a particle in the slow diffusion case scales as $N^{(av)}/\beta$. One can consider two weakly connected particles as a limiting case of one composite particle with two regions that have slow mass exchange between them. It means one can apply the variation estimation to Δc_{ip}. Substituting it all into (96) and noting that $L \sim \sqrt{S}$, one obtains:

$$\delta_3 \sim \frac{l_{ip}}{L} \frac{1}{\rho}. \tag{98}$$

Our estimates based on the numerical results in Traskunov and Latz [21] showed that, for the electrode and the C-rate in Latz and Zausch [19], $\rho \sim 1$, so one can reliably treat the particles there as separate from each other.

On the face of it, one may assume that the conditions of eDFN applicability analyzed in this Subsection hold almost always for realistic microstructures and cell operation regimes, as we noticed at the beginning of the Section; and, as in the case of formula (94), they are partially entangled with the u-homogenization conditions. It is, however, important to remember that all the estimates here are conditioned upon the criteria of stability introduced in Section 4.1: namely, that β is non-negative and positive at least in some parts of the interface. Also, one has to keep in mind that the solution of eDFN model may give a better approximation for one variables and a worse one for another. The singularity near $\rho \quad 0$ may start to affect the accuracy of c_s before that of u due to the fact that the right side of (91) remains bounded.

5. Linearized eDFN

In this Section, we aim at getting a further simplification of the homogenized cell model (42)–(46) called the linearized eDFN which was used to conduct the theoretical analysis of the local fluctuations in the electrodes in Traskunov and Latz [20,21]. In linearized eDFN, the additional new assumption that we make is that the kinetic law of the intercalation reaction can be sufficiently well approximated by a linear function at any moment of time.

Our presentation here strongly mirrors the one in Section 4; although the new approximation is distinct, the derivation methodology and the mathematical results are formally close. We introduce the variables with superscripts (ln) for the solutions of linearized eDFN. The linearized version of the intercalation kinetics is:

$$i_0^{(ln)}(u, c_s) \quad i_0(u, \widetilde{c_s}) + \beta(u, \widetilde{c_s}) \cdot (c_s \quad \widetilde{c_s}). \tag{99}$$

β is defined according to (56). $\widetilde{c_s}$ is a reference concentration level that itself is defined as the following surface average on the particle interface ($\widetilde{\beta}$ is defined according to (68)):

$$\widetilde{c_s} \quad \int_{\partial G_p} \frac{dS}{S} \widetilde{\beta} c_s. \tag{100}$$

Note that, with such definition, the total current through the interface is always

$$S \cdot \overline{i_0^{(ln)}}|_S \quad S \cdot \overline{N}|_S \Big/ F \quad \int dS \cdot i_0(u, \widetilde{c_s}). \tag{101}$$

The linearized eDFN equations, similar to (50)–(54), are:

$$\frac{\partial u_i^{(ln)}}{\partial t} \quad \overrightarrow{\nabla} \left(\sum_j \alpha_{ij} \overrightarrow{\nabla} u_j^{(ln)} \right) + a N_i^{(av)} \left(u^{(ln)} \right) \left[c_s^{(ln)} \right] \tag{102}$$

or

$$0 \quad \overrightarrow{\nabla} \left(\sum_j \alpha_{ij} \overrightarrow{\nabla} u_j^{(ln)} \right) + a N_i^{(av)} \left(u^{(ln)} \right) \left[c_s^{(ln)} \right], \tag{103}$$

$$N_i^{(av)} \left(u^{(ln)} \right) \left[c_s^{(ln)} \right] \quad \sum_p \frac{S^{(p)}}{S_{CV}} \overline{N_i}^{(p)}|_S \left(u^{(ln)}, \widetilde{c_s}^{(ln)(p)} \right), \tag{104}$$

$$\frac{\partial c_s^{(ln)}}{\partial t} \quad \overrightarrow{\nabla} \left(D_s \overrightarrow{\nabla} c_s^{(ln)} \right), \tag{105}$$

$$D_s \overrightarrow{\nabla} c_s^{(ln)} \cdot \overrightarrow{n}_{pe} \Big|_{\partial G_p} \quad \frac{1}{F} i_0 \left(u^{(ln)}, \widetilde{c_s}^{(ln)} \right) + \\ + \frac{1}{F} \beta \left(u^{(ln)}, \widetilde{c_s}^{(ln)} \right) \cdot \left(c_s^{(ln)} \quad \widetilde{c_s}^{(ln)} \right). \tag{106}$$

In (104), we made use of the fact that all N_i are proportional to i_0, hence the rule (101) is applicable and $\overline{N_i}|_S$ depends only on the concentration level $\widetilde{c_s}$. Also, here we used an additional index (p) to enumerate the particles in a given CV; thus the CV-averaged fluxes $N_i^{(av)}$ are the weighted sums of the particle-interface averaged fluxes $\overline{N_i}^{(p)}|_S$. As in the case of eDFN, boundary condition (106) is defined on the interface of one particle ∂G_p (see Fig. 1, right side), not of the whole active material domain, and (105) and (106) constitute a PDE subproblem defined on

each particle domain. For its equations, we do not use the subscript (p). Although it might cause confusion here, below, as in Section 4, we will mainly concentrate on the separate one-particle problem, do not keep the additional subscript and remove it here for consistency.

5.1. Mathematical properties of the linearized eDFN equations

Similarly to (59) and (60), we will use the following notations for the particle PDE subproblem (105) and (106):

$$\frac{\partial c_s^{(ln)}}{\partial t} \quad \vec{\nabla}\left(D_s \vec{\nabla} c_s^{(ln)}\right), \tag{107}$$

$$D_s \vec{\nabla} c_s^{(ln)} \cdot \vec{n}_{pe}\Big|_{\partial G_p} \quad N_0 + \frac{1}{F}\beta \cdot \left(c_s^{(ln)} \quad \widetilde{c}_s^{(ln)}\right), \tag{108}$$

$$N_0 \quad \frac{1}{F} i_0\left(u^{(ln)}, \widetilde{c}_s^{(ln)}\right). \tag{109}$$

As before, we aim at deriving the properties of the general solution from the properties of the stationary solutions by demonstrating the stability characteristics. The problem is however different from (59), (60), which was used as a reference in Section 4.1, due to the term $c_s^{(ln)} \quad \widetilde{c}_s^{(ln)}$, which also makes it an integro-differential problem following the definition (100). To recover the necessary stability properties, we introduce new variables:

$$c_s{}^{(ln)} \quad \overline{c} + c^f, \tag{110}$$

$$\overline{c} \quad \int \frac{dV}{V} c_s{}^{(ln)} \Rightarrow \int \frac{dV}{V} c^f \quad 0. \tag{111}$$

$\overline{c}$ represents the average SOC of the particle, c^f - the fluctuations relative to this average. Eqs. (107) and (108) turns into

$$\frac{\partial c^f}{\partial t} \quad \vec{\nabla}\left(D_s \vec{\nabla} c^f\right) \quad \frac{S}{V}\overline{N}|_S, \tag{112}$$

$$D_s \vec{\nabla} c^f \cdot \vec{n}_{pe}\Big|_{\partial G_p} \quad N_0 + \frac{1}{F}\beta \cdot \left(c^f \quad \widetilde{c}^f\right), \tag{113}$$

$$\frac{\partial \overline{c}}{\partial t} \quad \frac{S}{V}\overline{N}|_S. \tag{114}$$

If one treats N_0, D_s and β as external parameters $\vec{\theta}$ in the sense of Section 4.1, the dynamical system (112) and (113) has a unique stable equilibrium that is the solution of

$$0 \quad \vec{\nabla}\left(D_s \vec{\nabla} c^f\right) \quad \frac{S}{V}\overline{N}|_S, \tag{115}$$

$$D_s \vec{\nabla} c^f \cdot \vec{n}_{pe}\Big|_{\partial G_p} \quad N_0 + \frac{1}{F}\beta \cdot \left(c^f \quad \widetilde{c}^f\right). \tag{116}$$

The uniqueness is due to the condition on c^f (111). The asymptotic stability can be demonstrated, for example, by using the Lyapunov's second method (see Section 4.1): applying direct time differentiation, one can prove that the following functional is a Lyapunov function of the dynamical system:

$$V \quad \frac{1}{2}\int dV D_s \left|\vec{\nabla} c^f\right|^2 + \frac{1}{2}\int dS \frac{1}{F}\beta \cdot \left(c^f \quad \widetilde{c}^f\right)^2 \quad \int dS N_0 \cdot c^f + C, \tag{117}$$

that strictly decreases unless the stationary state is reached. C is a constant to be chosen for V to accurately satisfy Lyapunov's criteria.

After having established these facts, we can proceed with the next logical steps almost exactly replicating the approach in Section 4.1, with the exception of the variable substitution (110). The equilibrium (115) and (116) is similarly proved to be structurally stable, and the solution evolution adjusts itself continuously with the parameter (N_0, β, D_s) change. We assume that when not exactly the stationary one, the real dynamic solution for c^f tends to gravitate to it, and, for the purpose of our analysis, the scale of the dynamic solution variation can be estimated as the scale of the stationary solutions. The arguments in support of this approximation as well as the comments about the conditions under which they hold remain the same as in the last two paragraphs of Section 4.1.

Following the blueprint of Section 4.2, we reformulate the stationary problem in terms of the dimensionless parameters (68) and (69), with an addition of the new one $\widetilde{N_0} \quad N_0/\overline{N}|_S$. It leads us to the general solution in the form

$$c^f \quad \frac{L \cdot \overline{N}|_S}{\overline{D_s}|_V} \cdot f^{(3)}(\widetilde{\vec{x}}, \rho, \ldots), \tag{118}$$

where $f^{(3)}(\ldots)$ is a new dimensionless function. To investigate the asymptotic case $\rho \to +\infty$, we substitute the negative power series of ρ, like (76), into the stationary problem. The resulting sequence of PDEs and the boundary conditions are:

$$1 \quad \widetilde{\vec{\nabla}}\left(\widetilde{D_s}\widetilde{\vec{\nabla}} f_0^{(3)}\right), \tag{119}$$

$$\widetilde{\beta}\left(f_0^{(3)} \quad \widetilde{f}_0^{(3)}\right)|_{\partial G_p} \quad 0, \tag{120}$$

$$0 \quad \widetilde{\vec{\nabla}}\left(\widetilde{D_s}\widetilde{\vec{\nabla}} f_n^{(3)}\right), n > 0, \tag{121}$$

$$\widetilde{\beta}\left(f_1^{(3)} \quad \widetilde{f}_1^{(3)}\right)|_{\partial G_p} \quad \widetilde{N_0} \quad \widetilde{D_s}\widetilde{\vec{\nabla}} f_0 \cdot \vec{n}_{pe}, \tag{122}$$

$$\widetilde{\beta}\left(f_n^{(3)} \quad \widetilde{f}_n^{(3)}\right)|_{\partial G_p} \quad \widetilde{D_s}\widetilde{\vec{\nabla}} f_{n\ 1} \cdot \vec{n}_{pe}, n > 1. \tag{123}$$

$\widetilde{f}_n^{(3)}$ denotes $f_n^{(3)}$ averaged according to the rule (100). To make the solutions unique, one has to add the constraints following from (111):

$$\int dV f_n^{(3)} \quad 0. \tag{124}$$

Although the presence of the constants $\widetilde{f}_n^{(3)}$ makes the problems from the sequence integro-differential, in practice they can be solved as problems for differential equations, and $\widetilde{f}_n^{(3)}$ are fixed by the requirement that the solutions exist and that (124) holds.

For the case $\rho \to +0$, we substitute the positive power series for $f^{(3)}$ into the stationary PDE problem. Unlike in (81), there is no need to add a singularity term similar to g to get the PDE problems with existing solutions. The PDE problem sequence is:

$$1 \quad \widetilde{\vec{\nabla}}\left(\widetilde{D_s}\widetilde{\vec{\nabla}} f_0^{(3)}\right), \tag{125}$$

$$\widetilde{D_s}\widetilde{\vec{\nabla}} f_0^{(3)} \cdot \vec{n}_{pe}\Big|_{\partial G_p} \quad \widetilde{N_0}, \tag{126}$$

$$0 \quad \widetilde{\vec{\nabla}}\left(\widetilde{D_s}\widetilde{\vec{\nabla}} f_n^{(3)}\right), n > 0, \tag{127}$$

$$\widetilde{D_s}\widetilde{\vec{\nabla}} f_n^{(3)} \cdot \vec{n}_{pe}\Big|_{\partial G_p} \quad \widetilde{\beta}\left(f_{n\ 1}^{(3)} \quad \widetilde{f}_{n\ 1}^{(3)}\right), n > 0. \tag{128}$$

Here again, $\widetilde{f}_n$ can be found by taking the solution existence criteria and (124) into account.

Using these series, one can list the following properties of the stationary solution. First, when $\rho \to +0$, the gradient profile of concentration converges to a solution that does not depend on β. When $\rho \to +\infty$, there is also a finite and generally non-zero limit, but, as long $\beta \neq 0$

everywhere, the fluctuations on the interface are always zero because of the condition (120). That means that the correct asymptotic behavior of the surface standard deviation is this case is

$$\delta c_s^{(ln)}|_S \quad \left(\int \frac{dS}{S} \left(c_s^{(ln)} \quad \overline{c_s^{(ln)}}|_S \right)^2 \right)^{1/2} \sim \frac{L \cdot \overline{N}|_S}{\overline{D_s}|_V} \frac{1}{\rho} \quad \frac{\overline{N}|_S}{\overline{\beta}|_S}, \qquad \overline{c_s^{(ln)}}|_S \quad \int \frac{dS}{S} c_s^{(ln)}. \tag{129}$$

These results were used in the theory section in Traskunov and Latz [20]. As before, in line with our interpretation of parameter ρ given in Section 4.2, big values of ρ mean domination of the reaction negative feedback over diffusion in smoothing of the local concentration fluctuation on the interface. Although we are not aware of any rigorous proof of that fact, the numerical tests with different spheroid particle shapes in Traskunov and Latz [20] suggest that, in this geometry class, $\delta c_s^{(ln)}|_S$ depends inversely on ρ not only asymptotically but at almost any ρ. Overall, if one writes the formulas for $\delta c_s^{(ln)}|_S$ in both asymptotic cases using notation with physical dimensions, $\overline{\beta}|_S$ and $\overline{D_s}|_V$ appear always in the denominator. It emphasizes the role of the diffusion and of the negative reaction feedback as two forces that drive down the scale of the surface concentration fluctuations, non-spherical particle shape or any other factor destroying the microscopic isotropy being the forces that, to the contrary, drive the fluctuations up.

A closer look at the above formulas reveals interesting facts about the linearized eDFN and about the general mathematical assessment of DFN as a limit for the microscopic cell models. An important special case of particle geometry is sphere, with all other parameters being isotropic. Note that in this case always $\delta c_s^{(ln)}|_S \quad 0$ due to the spherical symmetry of the solution, and linearized eDFN (and eDFN as well) gives the solutions exactly identical to DFN. The purely geometrical effect of shape's deviation from sphere is encoded in the omitted dimensionless proportionality coefficient in (129) (and indirectly in function $f^{(3)}(\ldots)$). The overall physical scale of the fluctuations is encoded by the quantity with the dimension of concentration $L \cdot \overline{N}|_S / (\overline{D_s}|_V)$. After a few algebraic manipulations, it can be rewritten as follows:

$$\frac{L \cdot \overline{N}|_S}{\overline{D_s}|_V} \quad c_{\max} \frac{\overline{N}|_S}{N_{cr}} \quad c_{\max} \frac{\tau_{diffusion}}{\tau_{charge}}. \tag{130}$$

Here, $c_{\max}$ is the maximum possible lithium concentration in the given active material, N_{cr} is the critical flux level that can induce ion depletion and that can be estimated as $D_s c_{\max}/L$. This flux value defines one of the typical LIB C-rate limitations whose breaking can lead to a battery failure. $\tau_{diffusion} \quad L^2/\overline{D_s}|_V$ is the active material diffusion time, τ_{charge} is the time needed to charge the particle from 0% to 100% with constant average interface flux $\overline{N}|_S$. For the galvanostatic charging protocol, $\tau_{diffusion}$ can be associated with τ_{micro} and τ_{charge} - with τ_{macro} from formula (28). Now one can see that C-rate approaching the critical value is in fact identical to the homogenization parameter δ_2 for the active material diffusion case becoming not small, as we already mentioned in Section 2.2. Furthermore, relations (130) show that in this case $\delta c_s^{(ln)}|_S \sim c_{\max}$. While making this estimate, one has to keep in mind that the geometry-induced proportionality coefficient may vary (it's about 10% in the cases considered in Traskunov and Latz [20], although the geometry may visually seem distinctly non-spherical); also, the assumptions behind linearized eDFN model may not be valid anymore with big $\delta c_s^{(ln)}|_S$ (see the arguments in the next Subsection). With all these caveats, we have obtained an important result using only theoretical means: the local surface fluctuations of c_s do not disappear with the partial homogenization of variables u and are actually closely connected to the breakup of the homogenization conditions for the transport in active material (δ_2); and, from the battery system design point of view, both of this regimes are associated with high power battery applications that are required in many areas. The degree to which the local fluctuations of c_s are important cannot be assessed as a part of the general theoretical framework; it should be analyzed numerically in a case-by-case manner instead. But we can claim however that the one-particle system analysis in stationary regimes is sufficient, in many cases in its linearized version, in which the shape-relevant variables $f^{(3)}$ are completely decoupled from the parameters with dimension.

One can see that narrowing down the analysis to linearized eDFN allows one to obtain a bulk of important theoretical rigorous results about the properties of the localized gradient buildup in the active material particles, about their contribution to the localized interface fluctuations and about the general limitations of DFN. Note that the high C-rate-related limitations play an important role here again, as it did in the stationary approximation justification in Section 4.1.

5.2. Linearized eDFN: model applicability criterion

We continue following the logic of Section 4.3, to formulate the accuracy criteria, we can define the difference between eDFN solutions and the linearized eDFN solutions as the variables with superscript $(ln, 1)$:

$$u^{(en)} \quad u^{(ln)} + u^{(ln,1)}, \tag{131}$$

$$c_s^{(en)} \quad c_s^{(ln)} + c_s^{(ln,1)}. \tag{132}$$

The equations for $c_s^{(ln,1)}$ and $u^{(ln,1)}$, assuming that the former are small, can be obtained through subtraction of the linearized eDFN equations from the eDFN equations and through the subsequent linearization of the $c_s^{(ln,1)}$- and $u^{(ln,1)}$-dependent functions. In the end, for $c_s^{(ln,1)}$, one obtains the equations that are identical to (59) and (60), but with a different δN, that this time consists of all the non-linea terms we dropped from (99):

$$\delta N \quad \frac{1}{2F} \frac{\partial^2 i_0}{\partial c_s^2} (c_s \quad \widetilde{c_s})^2 + \ldots. \tag{133}$$

Due to this formal analogy, from this point on, the analysis follows exactly the presentation in Sections 4.1 and 4.3, almost all the comments and remarks made there remaining valid. The necessary linearized eDFN applicability criterion requires that δN is smaller than $\overline{N}|_S$, with $(c_s \quad \widetilde{c_s})^2$ being estimated according to the formulas of the previous Subsection. No singularity near $\rho \quad 0$ plays any role here, contrary to the eDFN case.

5.3. Linearized eDFN: numerical analysis of the accuracy realative to eDFN

Among the approximation steps derived and analysed in this paper, it is the transition between eDFN and linearized eDFN that has not been investigated numerically yet: in the numerical simulation results from Traskunov and Latz [21], eDFN was compared directly with a reduced-order model based on linearized eDFN and demonstrated remarkable accuracy in representing local c_s gradients, both in the sense of integral measures and point-wise, thus omitting the in-between step of comparing the two exact models directly. Here a missing direct numerical investigation-based comparison is presented.

To this end, we numerically solved both models for the galvanostatic/CC charging problem. The active material domain is represented by one particle in the shape of a spheroid with the aspect ratio 0.5. The main axis of the spheroid is 10 μm. The physical parameters of the simulation are given in Table 1. The Butler–Volmer kinetics (13) is used, and $c_s^{(\max)}$ in the Table denotes the corresponding active material saturation lithium density from the formula. The OCV as a function of SOC is

Table 1
Parameter set used in the microstructure simulation.

Parameters/units	Value
T/K	298.15
$c_s^{(initial)}/\mathrm{mol/cm^3}$	2.639×10^{-3}
$c_s^{(max)}/\mathrm{mol/cm^3}$	2.4681×10^{-2}
$D_s/\mathrm{cm^2\,s^{-1}}$	10^{-10}
$c_e/\mathrm{mol/cm^3}$	1.2×10^{-3}
$i_{00}/\mathrm{A/cm^2\,mol^{1.5}}$	0.002

$$
\begin{aligned}
U_0(SOC) \quad & 0.6379 + 0.5416\cdot\exp(-305.5309\cdot SOC) + \\
& +0.044\cdot\tanh(-(SOC-0.1958)/0.1088) \\
& -0.1978\cdot\tanh((SOC-1.0571)/0.0854) \\
& -0.6875\cdot\tanh((SOC+0.0117)/0.0529) \\
& -0.0175\cdot\tanh((SOC-0.5692)/0.0875)
\end{aligned}
\tag{134}
$$

The geometry and the parameters were used in the previous reports by the authors of the current research in Traskunov and Latz [20,21]. They roughly correspond to a graphite-based active material.

Here we mainly pay attention to high C-rates at which the lithium concentration gradients, whose prediction is one of the main concerns of the theory being developed, become especially pronounced. Two numerical experiments were done, with averaged current densities $\overline{i_0}|_S$ 10^{-4} A/cm^2 and $\overline{i_0}|_S$ 10^{-3} A/cm^2. They roughly correspond to the C-rates 2.6C and 26C (the actual C-rates reported for the cells whose active material is comprised of such particles will actually be higher if calculated according to the cutoff voltage, not according to the SOC criteria that we used here).

Tables 2 and 3 summarize the accuracy analysis. Here the evolution of two main quantities is tracked: of the accuracy-controlling parameter δ_3 (92) and of the ratio of the interface-localized difference between the eDFN-calculated concentration c_s and the liniarized eDFN-calculated concentration c_s to the surface fluctuations of c_s calculated according to eDFN. Here δN from the definition $\delta_3 \sim \delta N/N^{(av)}$ $\delta i_0|_S/\overline{i_0}|_S$ should be associated with the difference between N calculated according to both models; it was calculated either as total variance (difference between the maximum and the minimum) or as the standard deviation (STD). In the same vein, the ratio of the c_s correction to the c_s surface fluctuation was calculated both as the ratio of the total variances and as the ratio of the STDs.

A number of important observations can be drawn from this data. First, a small relative error in the representation of the surface fluctuations remains even at what is considered a high C-rate in the applications: the highest error value in the Tables is 5.4%. A snapshot of the lithium surface distribution per eDFN for the case $\overline{i_0}|_S$ 10^{-4} A/cm^2 at t 480 s is shown in Fig. 3 together with that of the difference between the distributions in eDFN and in linearized eDFN; the same color-to-value scale used in both plots helps assess the smallness of the difference relative to the surface fluctuations. Second, the error-controlling dimensionless parameter δ_3 remains indeed small as well, as per the theory from the subsection above. Finally, the relative error grows slower than the growth of the C-rate/N: when the latter is multiplied by 10, the former is multiplied by only 1.5–3.0, depending on the measures chosen.

Table 2
The time evolution of the accuracy characteristics of linearized eDFN vs. eDFN of the one-particle CC charge with the parameters from Table 1 and the geometry from Fig. 3 for the average current $\overline{i_0}|_S$ 10^{-4} A/cm^2. The further details and the explanation of the meaning of the table columns are in Section 5.3.

Time, s	Total var. $\delta N/N^{(av)}$	STD $\delta N/N^{(av)}$	Total var. $\delta c_s^{(error)}/\delta c_s$	STD $\delta c_s^{(error)}/\delta c_s$
120.0	0.019	0.005	0.015	0.013
240.0	0.030	0.009	0.031	0.029
360.0	0.007	0.002	0.015	0.016
480.0	0.038	0.012	0.016	0.013

Table 3
The time evolution of the accuracy characteristics of linearized eDFN vs. eDFN of the one-particle CC charge with the parameters from Table 1 and the geometry from Fig. 3 for the average current $\overline{i_0}|_S$ 10^{-3} A/cm^2. The further details and the explanation of the meaning of the table columns are in Section 5.3.

Time, s	Total var. $\delta N/N^{(av)}$	STD $\delta N/N^{(av)}$	Total var. $\delta c_s^{(error)}/\delta c_s$	STD $\delta c_s^{(error)}/\delta c_s$
12.0	0.124	0.008	0.035	0.044
24.0	0.077	0.019	0.045	0.035
36.0	0.117	0.019	0.027	0.037
48.0	0.178	0.013	0.052	0.054

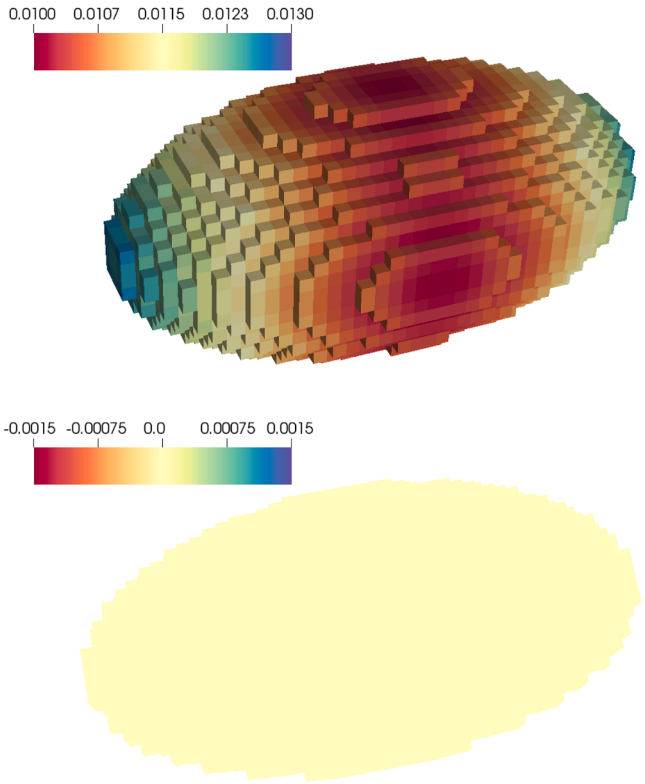

Fig. 3. Lithium distribution in the active material per eDFN (above) and the distribution difference between the simulation results of two models, eDFN and linearized eDFN (below). The parameters of the numerical simulation is from Section 5.3, with $\overline{i_0}|_S$ 10^{-4} A/cm^2, at t 480 s. The color bars denote the concentration in units [mol/cm^3].

The last observation may be a manifestation of a general trend. Indeed, if one combines together the formulas (92) and (133) with the asymptotic (129) and with the Butler–Volmer kinetics (13) (it specifies an implicit dependence of ρ on N/C-rate), one finds out that there is no clear power-law based asymptotic behaviour for the linearized eDFN error: different factors roughly offset each other. To which scale it is true for each particular case and from which point the asymptotic approximations fully sets in, should be decided with the help of numerical experiments. But the emergence of this trend for the realistic application-close set of parameters may be a good indication that there is no C-rate high enough for the linearized eDFN error to become practically noticeable.

6. Summary of the derivation methods, discussion

As mentioned above, there are common steps in the derivation of the

presented approximations in the two previous sections, which we want to repeat in non-technical terms to allow assessing the potential applicability of the ansatz beyond the basic cell model.

1. By analyzing spatial and time scale separation in a microscopic cell model, it is possible to separate the equations that formally allow the application of homogenization theory from those that do not.
2. For the equations that are not suitable for homogenization, approximations are identified that are better suited for rigorous theoretical analysis, yet are still accurate enough to capture the essential features of the full solution. In this paper, the linearized eDFN played this role.
3. For sufficiently slowly varying boundary conditions the approximate equations reduce the set of possible solutions to that of the stationary solutions and the ones close to them.

The correctness of every step is implicitly dependent on the steps that follow: the time-scale separation in the homogenized equations in point 1 holds if there is no process caused by the coupling to the non-homogenized part of the model, which is sufficiently fast to break the time scale separation. In our case, this is in turn guaranteed by the quasi-stationary dynamics in point 3.

The reduced-order model of Traskunov and Latz [21] utilizes all the points 1 to 3 and can be considered a next logical step in this framework. The linearization and the fact that the solutions are close to the quasi-stationary subset contributed strongly to the model's numerical efficiency. As was noted at the end of Section 2.1, inclusion of additional elements, such as side reactions or mechanics coupling, into the reduced-order model is possible, as long as the underlying mathematics is compatible with the points 1 to 3. Such model extensions can contribute to robust and first principle-based understanding of the cell dynamics and degradation, especially the extent of the influence of microstructural properties.

An interesting example for future qualitatively new applications of our strategy is the phase change electrodes described by Cahn–Hilliard-type models [32,33]. Cahn–Hilliard equations formulated as dynamic systems may lack the property of structural stability in certain situations, especially near the phase transition points. This can generate dynamics with the characteristics not fitting into the ones we derived in this paper. Yet, as it was argued [32], the underlying physics leading to the equations is intimately connected to the necessity to extend the classical DFN to incorporate the phenomena not observed in it, which is one of the reason the research presented here was conducted.

To sum up, one can thus see the importance of every element in our framework. To derive first principle-based upscaled cell models beyond the constraints formulated above additional instruments might be needed.

7. Conclusions

The paper gave a rigorous mathematical analysis of the transition between the microscopic continuous-medium lithium-ion cell model and the model based on an upscaled homogenized representation of the electrode porous medium. A special attention was given to the emergence of the spatially localized fluctuations of the cell variables that were previously reported in numerical and experimental studies and that are not captured by the standard classical widely used DFN model. As a byproduct of this analysis, we derived the (semi-)analytical laws which the localized fluctuations obey and that agree with the observations reported before in the literature (for example, Darling and Newman [13]), whose generality, however, was hard to assess, due to natural limitations of numerical analysis as opposed to it combined with analytical formulas. A number of critical parameters related to the general dynamics trends emerged from the derivation naturally (most importantly averaged surface current, ρ).

To the best of our knowledge, it is for the first time that a theoretical mathematics-based proof was demonstrated that the interface fluctuations under consideration (and potentially a number of other cell characteristics) do not disappear in general case in the microstructure homogenization limit often employed to justify the use of DFN. The importance of an accurate inclusion of the microstructure-relevant effects in the scientific analysis of the cell behavior was thus emphasized. We provided arguments in support of the close relation between the local fluctuations and the local anisotropic particle characteristics, such as non-spherical shape of the active material particles.

In our analysis, we moved through few stages, starting from the microscopic cell model and consequently introducing new approximations and testing the criteria of their applicability. Linearized extended DFN (eDFN) model emerged as the farthest model whose validity we can prove mathematically and support with the numerical experiments, and which combines high accuracy for realistic cell parameters with a big potential for obtaining closed-form analytical results. It can be used to accurately justify the use of the reduced-order DFN-like models reported earlier.

CRediT authorship contribution statement

Igor Traskunov: Methodology, Validation, Investigation, Software, Writing – original draft. **Arnulf Latz:** Conceptualization, Funding acquisition, Writing – review & editing.

Declaration of Competing Interest

The authors declare that they have no known competing financial interests or personal relationships that could have appeared to influence the work reported in this paper.

Data availability

The authors do not have permission to share data.

Acknowledgments

This work was funded by the Deutsche Forschungsgemeinschaft (German Research Foundation, DFG 281041241) in the framework of the research training group SiMET-Simulation of Mechanical, Electrical and Thermal Effects in Li-ion Batteries (281041241/GRK 2218).

References

[1] J. Newman, W. Tiedemann, Porous-electrode theory with battery applications, AIChE J. 21 (1) (1975) 25–41, https://doi.org/10.1002/aic.690210103.
[2] M. Doyle, T.F. Fuller, J. Newman, Modeling of galvanostatic charge and discharge of the lithium / polymer / insertion cell, J. Electrochem. Soc. 140 (6) (1993) 1526–1533.
[3] T.F. Fuller, M. Doyle, J. Newman, Simulation and optimization of the dual lithium ion insertion cell, J. Electrochem. Soc. 141 (1994) 1–10.
[4] M. Doyle, J. Newman, Design of lithium/ polymer battery systems, Electrochim. Acta 40 (13) (1995) 2191–2196.
[5] M. Doyle, J. Newman, A.S. Gozdz, C.N. Schmutz, J.M. Tarascon, Comparison of modeling predictions with experimental data from plastic lithium ion cells, J. Electrochem. Soc. 143 (1996) 1890–1903.
[6] P.D. Vidtst, R.E. White, Governing equations for transport in porous electrodes, J. Electrochem. Soc. 144 (4) (1997) 1343–1353.
[7] C.Y. Wang, W.B. Gu, B.Y. Liaw, Micro-macroscopic coupled modeling of batteries and fuel cells. {I.} model development, J. Electrochem. Soc. 145 (1998) 3407–3417.
[8] V. Taralova, O. Iliev, Y. Efendiev, Derivation and numerical validation of a homogenized isothermal Li-ion battery model, J. Eng. Math. 101 (2016) 1–27, https://doi.org/10.1007/s10665-015-9842-6.
[9] V. Taralova. Upscaling Approaches for Nonlinear Processes in Lithium-Ion Batteries, Technische Universitat Kaiserslautern, 2015. Ph.D. thesis.http://nbn-resolving.de/urn:nbn:de:hbz:386-kluedo-40860
[10] F. Ciucci, W. Lai, Derivation of micro/macro lithium battery models from homogenization, Transp. Porous Media 88 (2) (2011) 249–270, https://doi.org/10.1007/s11242-011-9738-5.

[11] B. Yan, C. Lim, L. Yin, L. Zhu, Three dimensional simulation of galvanostatic discharge of $LiCoO_2$ based on X-ray nano-CT images, J. Electrochem. Soc. 159 (10) (2012) A1604–A1614, https://doi.org/10.1149/2.024210jes.
[12] A.G. Kashkooli, E. Foreman, S. Farhad, D.U. Lee, K. Feng, G. Lui, V. De Andrade, Z. Chen, Morphological and electrochemical characterization of nanostructured $Li_4Ti_5O_{12}$ electrodes using multiple imaging mode synchrotron X-ray computed tomography, J. Electrochem. Soc. 164 (12) (2017) A2861–A2871, https://doi.org/10.1149/2.0101713jes.
[13] R. Darling, J. Newman, Modeling a porous intercalation electrode with two characteristic particle sizes, J. Electrochem. Soc. 144 (12) (1997) 4201–4208, https://doi.org/10.1149/1.1838166.
[14] M. Ender, An extended homogenized porous electrode model for lithium-ioncell electrodes, J. Power Sources 282 (2015) 572–580, https://doi.org/10.1016/j.jpowsour.2015.02.098.
[15] A. Schmidt, E. Ramani, T. Carraro, J. Joos, A. Weber, M. Kamlah, E. Ivers-Tiffée, Understanding deviations between spatially resolved and homogenized cathode models of lithium-ion batteries, Energy Technol. 9 (6) (2021) 2000881, https://doi.org/10.1002/ente.202000881.
[16] S.J. Harris, A. Timmons, D.R. Baker, D.R. Monroe, Direct in situ measurements of Li transport in Li-ion battery negative electrodes, Chem. Phys. Lett. 485 (4) (2010) 265–274, https://doi.org/10.1016/j.cplett.2009.12.033.
[17] S.J. Harris, E.K. Rahani, V.B. Shenoy, Direct in situ observation and numerical simulations of non-shrinking-core behavior in an MCMB graphite composite electrode, J. Electrochem. Soc. 159 (9) (2012) A1501–A1507, https://doi.org/10.1149/2.055209jes.
[18] D. Burow, K. Sergeeva, S. Calles, K. Schorb, A. Borger, C. Roth, P. Heitjans, Inhomogeneous degradation of graphite anodes in automotive lithium ion batteries under low-temperature pulse cycling conditions, J. Power Sources 307 (2016) 806–814, https://doi.org/10.1016/j.jpowsour.2016.01.033.
[19] A. Latz, J. Zausch, Multiscale modeling of lithium ion batteries : thermal aspects, Beilstein J. Nanotechnol. 6 (2015) 987–1007, https://doi.org/10.3762/bjnano.6.102.
[20] I. Traskunov, A. Latz, Localized fluctuations of electrochemical properties in porous electrodes of lithium-ion batteries: beyond porous electrode theory, Electrochim. Acta 379 (2021) 138144, https://doi.org/10.1016/j.electacta.2021.138144.
[21] I. Traskunov, A. Latz, New reduced-order lithium-ion battery model to account for the local fluctuations in the porous electrodes, Energy Technol. 9 (6) (2021) 2000861, https://doi.org/10.1002/ente.202000861.
[22] A. Latz, J. Zausch, Thermodynamic consistent transport theory of Li-ion batteries, J. Power Sources 196 (6) (2011) 3296–3302, https://doi.org/10.1016/j.jpowsour.2010.11.088.
[23] S. Hein, T. Danner, A. Latz, An electrochemical model of lithium plating and stripping in lithium ion batteries, ACS Appl. Energy Mater. 3 (9) (2020) 8519–8531, https://doi.org/10.1021/acsaem.0c01155.
[24] P. Arora, M. Doyle, R.E. White, Mathematical modeling of the lithium deposition overcharge reaction in lithium-ion batteries using carbon-based negative electrodes, J. Electrochem. Soc. 146 (10) (1999) 3543–3553.
[25] J. Christensen, J. Newman, A mathematical model of stress generation and fracture in lithium manganese oxide, J. Electrochem. Soc. 153 (6) (2006) A1019–A1030, https://doi.org/10.1149/1.2185287.
[26] V. Jikov, S. Kozlov, O. Oleinik, G. Yosifian, Homogenization of Differential Operators and Integral Functionals, Springer, 1994.
[27] W. Lai, F. Ciucci, Mathematical modeling of porous battery electrodes-revisit of Newman's model, Electrochim. Acta 56 (11) (2011) 4369–4377, https://doi.org/10.1016/j.electacta.2011.01.012.
[28] V. Vladimirov, Equations of Mathematical Physics, second ed., Mir Publishers, 1983.
[29] I. Prigogine, G. Nicolis, Self-Organization in Nonequilibrium Systems. From Dissipative Structures to Order through Fluctuations, J. Wiley & Sons, New York, 1978.
[30] K.R. Brownstein, C.E. Tarr, Importance of classical diffusion in NMR studies of water in biological cells, Phys. Rev. A 19 (1979) 2446–2453, https://doi.org/10.1103/PhysRevA.19.2446.
[31] S. Hein, J. Feinauer, D. Westhoff, I. Manke, V. Schmidt, A. Latz, Stochastic microstructure modeling and electrochemical simulation of lithium-ion cell anodes in 3d, J. Power Sources 336 (2016) 161–171, https://doi.org/10.1016/j.jpowsour.2016.10.057.
[32] B. Orvananos, T.R. Ferguson, H.-C. Yu, M.Z. Bazant, K. Thornton, Particle-level modeling of the charge-discharge behavior of nanoparticulate phase-separating Li-ion battery electrodes, J. Electrochem. Soc. 161 (4) (2014) A535–A546, https://doi.org/10.1149/2.024404jes.
[33] G.F. Castelli, L. von Kolzenberg, B. Horstmann, A. Latz, W. Dorfler, Efficient simulation of chemical-mechanical coupling in battery active particles, Energy Technol. 9 (6) (2021) 2000835, https://doi.org/10.1002/ente.202000835.